ELSEVIER

Chemical Geology 194 (2003) 81–104

CHEMICAL GEOLOGY
INCLUDING
ISOTOPE GEOSCIENCE

www.elsevier.com/locate/chemgeo

Melt inclusion geochemistry and computer modeling of trachyte petrogenesis at Ponza, Italy

L. Fedele[a,*], R.J. Bodnar[a], B. DeVivo[b], R. Tracy[a]

[a] *Department of Geological Sciences, Virginia Tech., Blacksburg, VA 24061, USA*
[b] *Dipartimento di Geofisica e Vulcanologia, Università di Napoli Federico II, 80134 Naples, Italy*

Received 17 January 2002; received in revised form 11 June 2002

Abstract

The Punta della Guardia trachytic unit on the island of Ponza, Italy is thought to represent the latest stage in the evolution of a parent basaltic melt in a shallow magma chamber undergoing fractional crystallization. To test this hypothesis, melt inclusions (MI) have been analyzed to constrain the crystallization history of the Ponza trachyte. The trachyte is a weakly porphyritic lava that contains phenocrysts of plagioclase, K-feldspar, clinopyroxene and biotite. Melt inclusions were observed and measured in plagioclase, clinopyroxene and K-feldspar. The crystallized devitrified melt inclusions were heated to dissolve (melt) the crystals, quenched to a homogeneous glass, and then analyzed for major elements by electron microprobe. Two different heating protocols, one involving rapid heating in a one-atmosphere furnace, and the other involving slower heating in a microscope heating stage, were used to homogenize the inclusions in order to investigate possible effects of heating rates on inclusion composition. No detectable difference was found. Melt inclusion compositions suggest that the magma evolved from an early phase dominated by clinopyroxene ± plagioclase crystallization to a late stage in which melt composition was controlled by precipitation of two feldspars.

The potential basaltic parent magma does not crop out on Ponza, although more primitive and coeval basalts and trachybasalts are found on nearby Ventotene Island, which is considered to be co-magmatic with Ponza. Using the program MELTS, we have compared results obtained from melt inclusions in the Ponza trachyte with melt compositions predicted for fractional crystallization of a magma having the composition of the Ventotene trachybasalt. Crystallization trends predicted by MELTS are consistent with data from melt and host phases, although differences in measured and predicted compositions are significant in some cases. In spite of these differences, the model results and measured compositions are consistent with the hypothesis of a genetic link between the magmatism of Ponza and Ventotene.

Keywords: Melt Inclusions; Trachyte; Ponza; MELTS

1. Introduction

Melt inclusions (MI) have proven to be a valuable tool to investigate the physico-chemical evolution of magmatic systems, from initial generation in the deep crust or mantle through all of the subsequent processes that operate during ascent and eruption onto the surface (Lowenstern, 1995; Hari et al., 1991; Sobolev, 1996). MI contain samples of melt trapped during crystallization of the magma, hence, major and trace element data obtained through MI analysis may be

* Corresponding author. Fax: +1-540-2313-386.
E-mail address: lfedele@vt.edu (L. Fedele).

0009-2541/02/$ - see front matter © 2002 Elsevier Science B.V. All rights reserved.
PII: S0009-2541(02)00272-3

used to constrain and understand petrogenetic processes including fractional crystallization, magma mixing, and contamination (Roedder, 1979; Lowenstern, 1995; Sobolev, 1996, Frezzotti, 2001).

Owing to its location in the Tyrrhenian sea, the island of Ponza, Italy offers the opportunity to investigate the formation of alkaline magmas generated in a complex geodynamic setting, specifically that of a basin undergoing extension within an overall collisional tectonic framework (Stanley and Wezel, 1985). We present a study of melt inclusions from Ponza, and combine analytical results from melt inclusions with compositional trends predicted by numerical models to investigate the role played by fractional crystallization of a basaltic magma in a shallow magma chamber in the origin of the trachytes on Ponza.

2. Geological setting

Ponza is the largest of the five islands of the Pontine archipelago, a 30-km-long chain located in the Gulf of Gaeta. The archipelago can be divided into two groups: Ponza, Palmarola and Zannone on the northwest, and Ventotene and Santo Stefano to the southeast (Fig. 1B). It is located at the intersection of the 41st parallel discontinuity and the Ortona-Roccamonfina line (Fig. 1A). The 41st parallel discontinuity is a dextral transcurrent fault system at the boundary between the northern and southern Tyrrhenian basin (Savelli and Wezel, 1979), whereas the Ortona-Roccamonfina line (Locardi, 1982) is a late Pliocene dextral strike-slip fault (Patacca et al., 1990), which represents the present-day boundary between the Central and Southern Apennines (Fig. 1A).

Ponza is located at the intersection of two domains that have undergone significantly different styles of tectonic evolution since the late Miocene. Because the rapid opening of the Tyrrhenian basin since late Tortonian times (~ 10–7 Ma) and the development of the arc-shaped thrust-belt mountain chain both occurred in a convergent tectonic setting, the evolution of the basin and the Apennine chain poses an interesting tectonic problem. Furthermore, while the northern Tyrrhenian basin underwent moderate extension, the southern experienced significant thinning of the lithosphere and the crust, and reached "close to oceanic characteristics" (Bassi et al., 1997).

Various models have been proposed to explain the formation of the Tyrrhenian sea and the Apennine chain. Boccaletti and Guazzone (1972) proposed that the Tyrrhenian sea represents a back-arc marginal basin in a trench–arc–back-arc system, which migrated from the northwest to reach its current position. In this model, the trench is located in the Ionian sea off the coast of Calabria, where the non-volcanic arc is Calabria itself and the Aeolian islands represent the volcanic arc. A concurrent counterclockwise rotation of the Corsica-Sardinia block is responsible for development of the Apennine chain (Fig. 1A).

A Benioff zone dipping to the northwest, evidenced by deep earthquake foci, has been suggested by Barberi et al. (1973). Laubscher (1975) and Scandone (1980) inferred the existence of two westward-dipping subduction zones, one located at the eastern margin of the Sardinia-Corsica block and the other at the western margin of the Adria microplate (Adriatic Sea area in Fig. 1A). More recently, Lavecchia and Stoppa (1996) proposed a new model for the tectonic evolution of the region. Based on the characteristics and distribution of volcanism around the Tyrrhenian basin and the discovery of carbonatitic volcanism, they proposed a passive rifting mechanism to explain the origin and evolution of the basin. Turco and Zuppetta (1998) examined the available geological and geophysical data and proposed a kinematic model of the area, which is consistent with a passive rifting mechanism.

Ponza is composed of two volcanic units, an older silica-rich (Pliocene) unit that occurs in the northern and central part of the island, and a younger (Pleistocene), alkali-potassic unit that is present only in the southern part of the island (Fig. 2; Bellucci et al., 1999). The older unit, composed of dikes and hyaloclastites of submarine origin, varies in composition from rhyolite to rhyodacite, and in the northernmost part of the island has been affected by an extensive hydrothermal alteration event, which caused deep kaolinitization and the formation of bentonite deposits (Pozzuoli, 1988; Ylagan et al., 1996). The younger volcanic products are trachytes, erupted and emplaced above sea level, which form pyroclastic sequences, scoria cones and lava flows. This study focuses on the Ponza trachytes representing the late stages of crystallization of volcanic rocks that are associated with

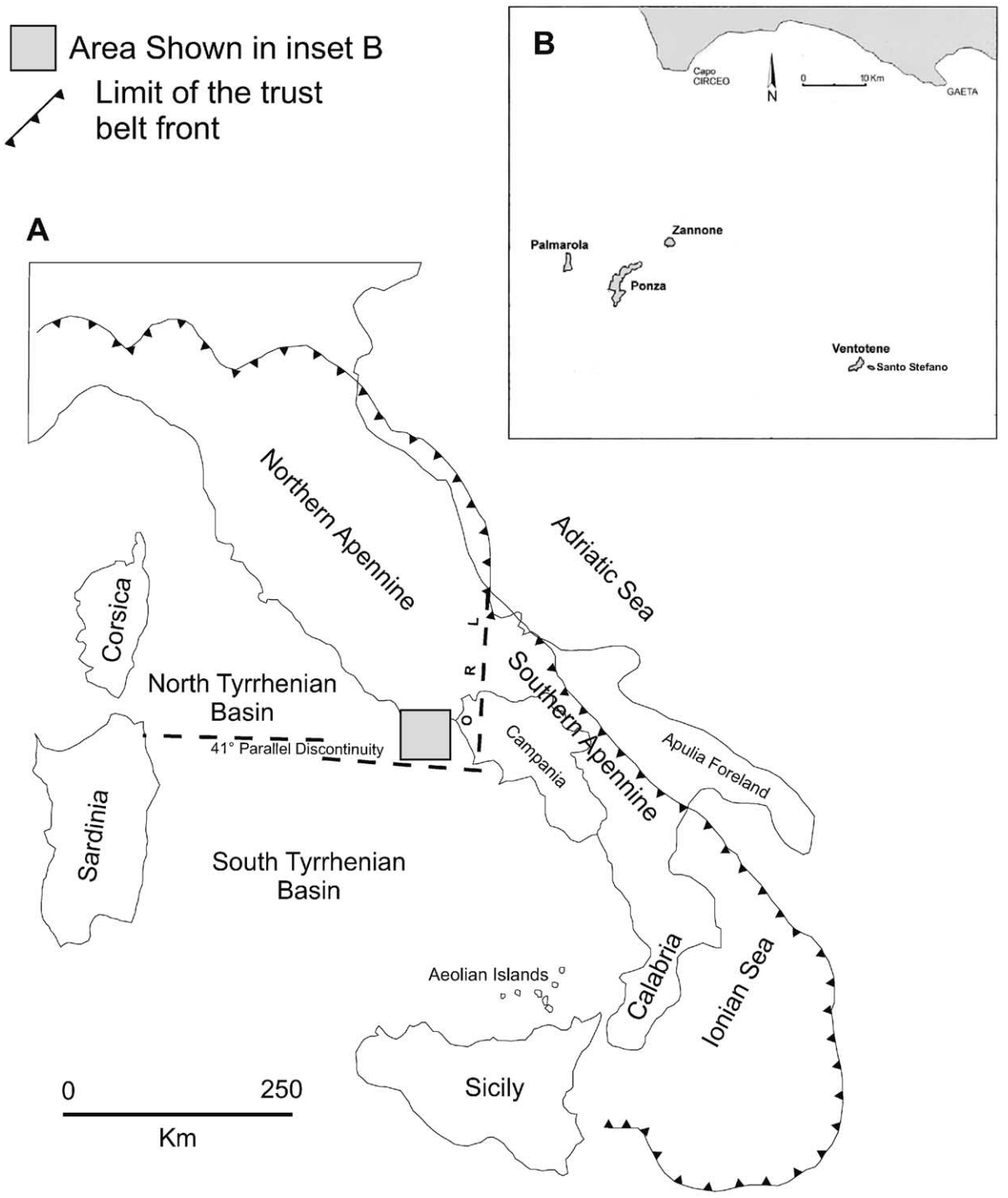

Fig. 1. (A) Schematic tectonic map of Italy showing the main tectonic blocks. The box outlines the region of the Pontine archipelago shown in the enlargement in (B). ORL = Ortona-Roccamonfina Line. (B) Location of Ponza and the Pontine archipelago.

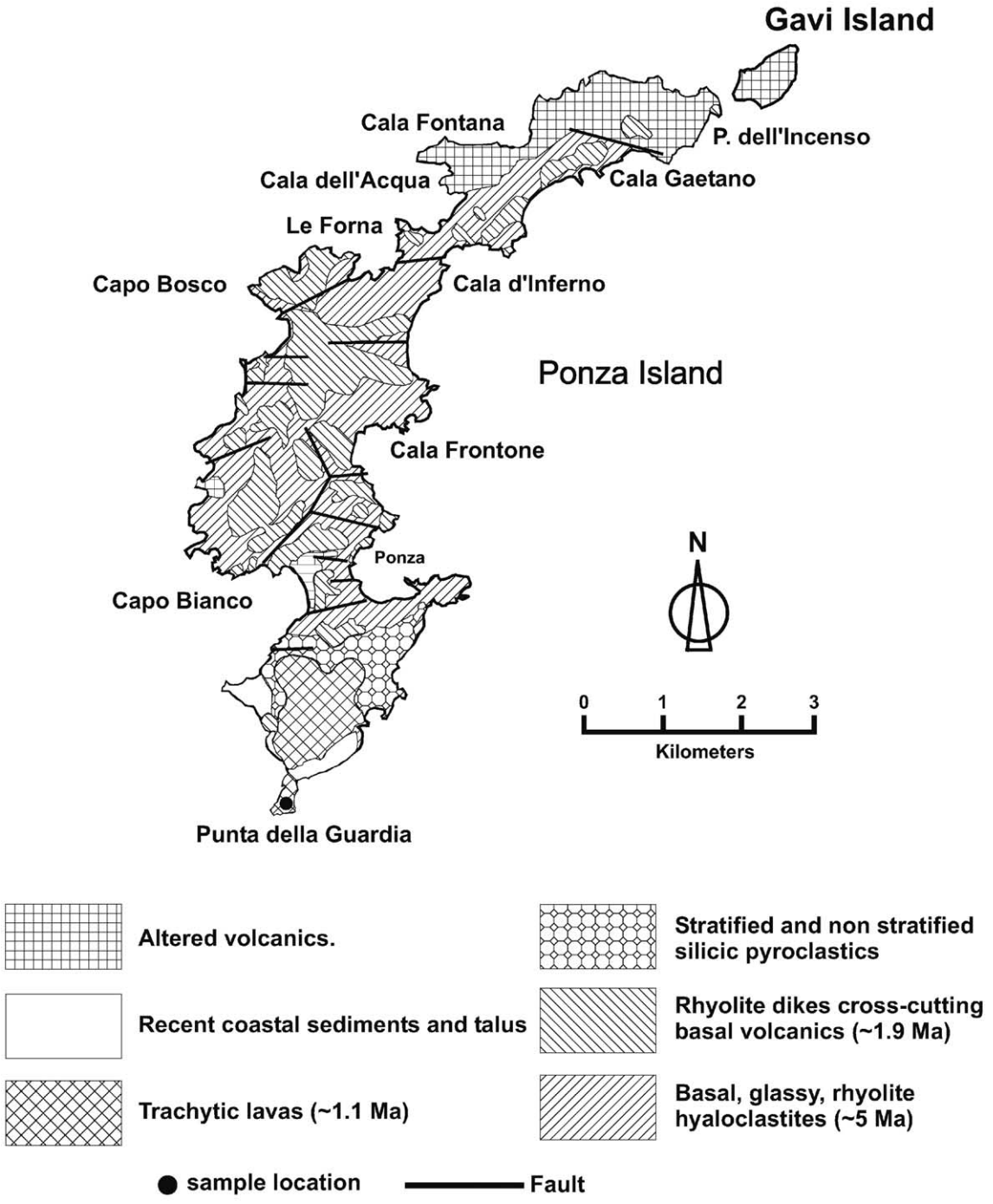

Fig. 2. Simplified geologic map of Ponza (after Bellucci et al., 1999).

the magmatism in the Campanian area (Conte and Dolfi, 2002; Fig. 1A).

3. Sample and melt inclusions description

Samples were collected from all of the volcanic units on Ponza, using the geologic map of Bellucci et al. (1999) to select sampling locations. Best-exposed and freshest outcrops occur on the steep cliffs along the coastline. Doubly polished thick sections approximately 200–300-μm thick were made from the collected samples and examined to search for phenocrysts containing melt inclusions suitable for analysis. Only the trachyte samples collected at Punta della Guardia (Fig. 2), which represents the more mafic (primitive) part of the Monte della Guardia trachyte (Conte and Dolfi, 2002), were found to contain useful MI.

The studied rock is porphyritic, with phenocrysts of normally zoned plagioclase (An_{46} to An_{87}), sanidine (Ab_{30} to Ab_{40}, with An < 10%), clinopyroxene (Di_{50} to Di_{69}), and biotite, in order of decreasing abundance. The phenocrysts range in size from 1 to 5 mm and always show abundant fractures. Melt inclusions large enough (>15 μm) for microthermometric and Electron Microprobe analysis were found mainly in plagioclase, and less commonly in pyroxene and alkali feldspars. The Ponza rhyolites are very fine-grained rocks with only rare, small (typically less than 1 mm) phenocrysts which contained scarce, small (< 10 μm) MI. They proved to be unsuitable for melt inclusion studies.

Melt inclusions (MI) in feldspars and pyroxene range in size from 5 to 50 μm, and their shape is generally spherical or elongated. They are always completely crystallized or devitrified and a bubble is always present, although it is usually not visible until melting begins during heating experiments. MI occur individually or in small clusters, not along fractures and can be considered primary. Commonly, they contain small opaque crystals, which melt during the heating runs.

A first attempt to extract phenocrysts from the trachyte by crushing proved unsuccessful due to the relatively small size of the crystals, which were also easily broken owing to the presence of numerous fractures. Hence, we extracted single crystals containing melt inclusions directly from the thin sections using a hand-held mini drill fitted with diamond bits and using a binocular stereo-microscope.

4. Analytical techniques

4.1. Homogenization of crystallized melt inclusions

MI in the Ponza trachytes required heating and quenching to obtain a homogeneous glass, as they are partially or totally recrystallized when found. Indeed, analyzing crystallized MI may generate misleading or useless information about the original melt composition and volatile content if they are not homogenized (Roedder, 1979; Raia et al., 2000). It should be noted, however, that recent advances in laser ablation ICP-MS allow in some cases reliable quantitative analyses of unhomogenized crystallized melt inclusions (Halter et al., in press).

Three different approaches are commonly used to reheat and homogenize crystallized melt inclusions. These include heating melt inclusions contained in doubly polished wafers, using a one-atmosphere stage mounted on a petrographic microscope (Sobolev, 1996), using a one-atmosphere furnace (Sinton et al., 1993; Nielsen et al., 1995), or heating the inclusions under high confining pressure in a cold-seal autoclave (Student and Bodnar, 1999; Thomas et al., 2000). Each of these techniques offers advantages and disadvantages, depending on the nature of the samples and the type of information sought (Lowenstern, 1994; Nielsen et al., 1998; Student and Bodnar, 1999; Yang and Bodnar, 1994).

Nielsen et al. (1998) report that a major disadvantage of the microscope heating stage technique is that extensive sample preparation is required, and that production of doubly polished sections can introduce microfractures that allow loss of volatiles or other components from the inclusions during heating. However, studies of fluid inclusions in soft and/or easily cleavable minerals such as calcite, fluorite and barite by various workers over the past few decades has led to the development of mineral-friendly sample preparation techniques to significantly minimize the introduction of microfractures during sample preparation (Bodnar and Bethke, 1984; Ulrich and Bodnar, 1988).

The presence of volatiles (e.g. H_2O) can also affect the behavior of melt inclusions during homogenization experiments if the volatiles diffuse out of the MI during heating (Roedder, 1984). This may produce melt inclusions with compositions different from that of the melt originally trapped. Sobolev et al. (1980) reported that slow heating rates can favor loss of volatiles through hydrogen diffusion. This, in turn, results in an increase in the final homogenization temperature, a different melting behavior and, most importantly, modified (incorrect) compositions of the MI. In this case, the duration of the heating event can be critical, and analysis of heated and un-heated MI can help to place constraints on the extent of volatile loss during heating (Raia et al., 2000).

One of the main advantages of studying melt inclusions in doubly polished wafers is that inclusions can be observed not only before and after, but also during heating (Danyushevsky et al., in press). Also, melt inclusions may trap solid phases along with the melt, and if these solids are incorporated back into the melt during heating, a wide range in melt compositions would result, with the variability being a function of the relative size of the trapped solid phases. If the inclusions are not observed before and during heating, the heterogeneous nature of the inclusions would not be recognized and the resultant range in MI compositions might be incorrectly interpreted to be the result of petrogenetic processes. However, in some cases, only compositional evidence, gained after analyses of MI, can be used to identify accidentally trapped mineral phases. For example, in the present study, compositional evidence (i.e. very high P content) suggests that apatite was trapped along with melt in some inclusions in clinopyroxene.

In order to observe the melting behavior of the inclusions, we used microscope-mounted heating stages with slow heating rates. During the experiments, no decrepitation phenomena were observed, hence, it was not necessary to heat the inclusions under pressure. To confirm that the slow heating rates did not affect the compositions and the melting behavior of the inclusions as reported by Sobolev et al. (1980; i.e. loss of H_2O), some short-duration heating experiments were conducted in a one-atmosphere furnace, and the results compared to the longer-duration experiments. However, even short-duration heating does not completely rule out the possibility that some water may be lost by diffusion during the experiments (Skirius et al., 1990; Qin et al., 1992; Lowenstern, 1994).

Melt inclusions were heated in either a high temperature (1500 °C) Linkam stage, or a Vernadsky heating stage (Sobolev et al., 1980), or a one-atmosphere furnace, until complete melting of all crystals was achieved. MI were quenched by removal from the furnace in the Linkam stage, by turning off the power to the Vernadsky stage, or by extraction from the one-atmosphere furnace followed by quenching in water. The quenching rates were consequently different. Whereas the Vernadsky stage allows an extremely fast quenching rate (<1 s) from high T (1200 °C) to <800 °C, the Linkam requires at best a few tens of seconds to cool over this same range. The 1-atm furnace allowed quenching from high T to room temperature in less than 3 s. We found no differences in temperatures of melting or melting behavior among MI heated in the Linkam stage, the Vernadsky stage or the 1-atm furnace.

All stage experiments were conducted in controlled (inert gas) atmosphere to avoid oxidation of the crystals. Nitrogen was used in the Linkam stage and high-purity helium that was de-oxygenated by passing over hot (600 °C) titanium metal powder was used in the Vernadsky stage. The heating rate for the Linkam stage was computer-controlled using the following heating schedule: 20 °C/min from 0 to 600 °C, 10 °C/min from 600 to 1000 °C, and 5 °C/min from 1000 °C to the final melting temperature. The Vernadsky stage is operated manually using a Variac, so the heating rate cannot be controlled precisely. The temperature was raised slowly over an extended period of time (~ 2–3 h) at an average rate of 5 °C/min. Both stages were calibrated using the melting points of NaCl (801 °C) and Au (1064 °C). The precision is ± 5 °C for the Linkam stage and ± 2 °C for the Vernadsky stage at 1000 °C (measured by thermocouple).

In order to test whether the slow heating rates used for the Ponza MI affected the compositions (Sobolev et al., 1980), some inclusions were homogenized using a one-atmosphere furnace in the Department of Earth and Planetary Sciences at the American Museum of Natural History in New York. MI in plagioclase and pyroxene crystals were placed into a

platinum capsule, one crystal per run, and introduced into the furnace by sliding the capsule into a quartz tube. The capsule was attached to a ceramic rod to allow for rapid extraction and quenching in water. The furnace was preheated to 1170 °C, based on step-heating runs carried out at the beginning of the experiments, which showed this to be the minimum temperature required to obtain complete melting of the MI. This temperature is in good agreement with the temperatures (1150–1200 °C) required for complete melting using the much slower heating rates in the microscope-mounted stages. To avoid oxidation, a few drops of immersion oil were placed in the capsule with the crystal according to the technique described by Thomas and Webster (2000). MI were kept at high temperature for 5 min and then quenched.

4.2. Electron microprobe analysis

Major element analyses for inclusions heated using the Linkam and the Vernadsky stages were performed on a CAMECA SX50 Electron Microprobe in the Department of Geological Sciences at Virginia Tech., using a 15-kV and 2-nA raster beam(5 μm). The low current was chosen to minimize loss of sodium from the glass through heating by the electron beam. Counting time was 20 s for F and Cl and 10 s for all other elements including Na, which was analyzed first. The Electron Microprobe was calibrated using synthetic and natural materials of known composition. Inclusions homogenized in the one-atmosphere furnace were analyzed at the American Museum of Natural History on a CAMECA SX100 Electron Microprobe using a 15-kV defocused beam (5 μm) and a current of 10 nA for all elements except Na, which was analyzed first using a 2-nA beam. Counting times were 80 s for F, 40 s for Cl and Na, 30 s for P and 20 s for all others elements. The instrument was calibrated using minerals of known composition. Only inclusions larger than 15 μm were used for EMPA analysis to avoid including any of the host phase in the analytical volume for the inclusion. A few larger inclusions were analyzed twice in different spots to test for homogeneity. These repeated analyses confirm that the heating experiments produced homogeneous glasses in the inclusions.

5. Results

During heating in the microscope stages, inclusions in plagioclase and K-feldspar showed no detectable melting below 1000 °C, and complete melting of the inclusions occurred between 1150 and 1200 °C. For MI in pyroxene, no melting was detected below 950 °C and complete melting occurred between 1150 and 1200 °C. MI did not noticeably change shape or size during heating, suggesting that relatively little material dissolved from the inclusion walls during the experiments (Fig. 3). However, it should be noted

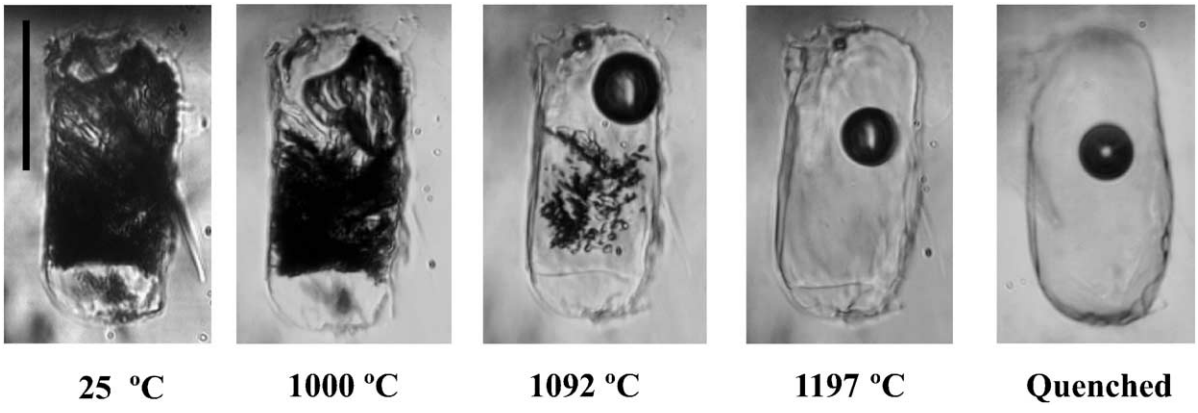

Fig. 3. Melting sequence of a crystallized melt inclusion in plagioclase. At room temperature, the inclusion consists of a mass of intergrown, fine-grained, crystals ± glass. By 1092 °C, most of the silicates have melted leaving only a mass of fine-grained opaques, which melt between 1092 and 1197 °C. After quenching, the inclusion contains a homogeneous glass and a vapor bubble. Black line is for scale and is 25 μm.

Table 1a
MI compositions

	K-feldspar MI			Plagioclase MI—heated with Linkam and Vernadsky stages														
	(1)-A	(1)-B	(1)-C	(1)-A	(1)-B	(2)-C	(2)-D	(1)-E	(1)-F	(1)-G	(2)-H	(1)-I	(1)-L	(1)-M	(1)-N	(2)-O	(1)-P	(1)-Q
SiO_2	59.67	59.94	55.92	57.30	57.91	59.14	60.07	61.78	60.68	59.38	58.15	58.18	57.39	57.60	56.29	57.89	57.69	57.61
TiO_2	0.02	0.03	0.08	0.71	0.64	0.82	0.69	0.65	0.67	0.56	0.39	0.55	0.45	0.68	0.72	0.43	0.36	0.37
Al_2O_3	18.61	18.40	17.93	20.39	20.18	20.30	19.05	19.11	19.32	21.62	21.95	20.89	21.68	21.14	20.03	21.51	22.25	22.61
MgO	1.04	0.96	1.43	0.72	0.75	0.75	0.62	0.57	0.65	0.44	0.44	0.48	0.45	0.65	0.70	0.41	0.35	0.33
CaO	6.98	6.83	9.56	3.44	2.96	3.43	2.76	2.39	2.70	3.64	3.59	3.39	3.64	3.17	3.30	3.51	4.36	4.49
MnO	0.33	0.32	0.89	0.05	0.10	0.13	0.11	0.12	0.15	0.06	0.10	0.16	0.09	0.06	0.14	0.12	0.06	0.14
FeO	2.36	2.35	2.40	4.08	3.83	4.15	3.68	3.31	3.40	2.94	2.58	2.75	2.51	3.58	4.01	2.51	2.45	2.48
Na_2O	4.26	4.25	4.10	4.57	5.18	3.13	4.29	3.27	3.60	4.07	5.27	4.61	5.00	4.97	5.31	5.71	5.72	5.60
K_2O	7.14	7.29	5.85	6.21	6.26	6.18	5.46	5.63	5.60	6.53	6.29	6.45	6.24	5.77	6.11	5.48	5.10	5.20
P_2O_5	0.02	0.05	0.15	0.27	0.29	0.33	0.83	0.77	0.79	0.27	0.16	0.22	0.12	0.28	0.24	0.20	0.14	0.21
F	0.41	0.00	0.00	0.14	0.15	0.24	0.21	0.21	0.24	0.18	0.34	0.20	0.06	0.16	0.20	0.20	0.12	0.11
Cl	0.00	0.01	0.03	0.18	0.15	0.17	0.02	0.01	0.01	0.23	0.23	0.20	0.14	0.16	0.18	0.15	0.16	0.12
Total	100.83	100.42	98.33	98.06	98.40	98.76	97.78	97.81	97.82	99.92	99.48	98.08	97.76	98.22	97.23	98.11	98.77	99.27

	Plagioclase MI—heated with Linkam and Vernadsky stages									Plagioclase MI—heated in one-atmosphere furnace							
	(1)-R	(1)-S	(1)-T	(1)-U	(1)-V	(1)-W	(1)-X	(1)-Y	(1)-Z	(1)-AA	(1)-AB	(2)-AC	(1)-AD	(1)-AE	(2)-AF	(1)-AG	(1)-AH
SiO_2	59.92	58.42	60.36	54.96	52.40	54.91	53.51	55.44	52.63	48.86	49.19	49.00	48.54	47.66	48.47	50.94	49.45
TiO_2	0.44	0.42	0.43	1.20	0.96	0.39	0.57	0.17	0.72	1.73	1.64	1.65	1.82	1.83	1.86	1.48	1.35
Al_2O_3	19.75	21.32	20.16	18.87	21.92	22.07	23.91	22.99	21.68	18.93	19.12	19.78	20.15	19.59	20.22	20.71	21.75
MgO	0.58	0.57	0.60	1.17	1.23	0.73	0.35	0.58	0.83	3.72	3.76	3.87	2.99	3.40	3.14	2.68	1.89
CaO	3.36	4.04	4.14	3.48	6.96	5.60	8.09	6.73	5.88	7.89	7.75	7.89	7.30	6.32	6.80	6.58	7.42
MnO	0.14	0.18	0.22	0.16	0.06	0.12	0.22	0.08	0.17	0.20	0.20	0.15	0.19	0.18	0.20	0.16	0.14
FeO	3.06	2.85	2.30	4.94	4.19	4.18	2.09	2.76	4.26	8.05	8.33	8.14	7.34	8.31	7.70	6.60	6.06
Na_2O	5.42	5.52	5.59	5.85	5.06	4.78	6.54	5.37	5.07	4.72	4.67	4.84	5.21	5.64	5.52	5.62	6.50
K_2O	5.83	5.39	6.01	4.92	3.98	3.27	2.92	3.68	4.62	3.51	3.41	3.36	4.27	4.37	4.27	4.53	4.25
P_2O_5	0.17	0.15	0.13	0.55	0.08	0.26	0.22	0.25	0.84	0.73	0.70	0.85	0.63	0.65	0.69	0.47	0.50
F	0.36	0.25	0.22	0.53	0.00	0.00	0.71	0.00	0.20	0.25	0.27	0.23	0.53	0.68	0.59	0.50	0.47
Cl	0.13	0.16	0.02	0.00	0.00	0.01	0.15	0.16	0.23	0.16	0.17	0.16	0.18	0.20	0.19	0.17	0.13
Total	99.15	99.27	100.17	96.63	96.84	96.32	99.26	98.20	97.11	98.74	99.22	99.92	99.16	98.82	99.65	100.43	99.91

CPX MI—heated with Linkam and Vernadsky stages

	(1)-A*	(1)-B*	(1)-C*	(1)-D	(1)-E*	(1)-F	(1)-G	(1)-H*	(1)-I	(1)-L	(1)-M*
SiO_2	46.49	56.47	50.86	57.77	39.62	44.40	54.79	50.28	51.26	52.42	51.23
TiO_2	0.56	0.52	0.99	0.90	0.64	4.02	0.32	0.60	0.30	0.58	0.49
Al_2O_3	9.83	13.92	12.33	16.04	7.59	10.74	11.23	10.29	11.47	10.97	12.56
MgO	5.64	2.42	4.06	3.29	5.69	4.41	4.93	5.74	6.08	5.75	4.20
CaO	14.81	7.84	17.48	6.52	18.28	10.81	10.46	11.53	10.41	10.43	10.78
MnO	0.39	0.29	0.05	0.38	0.31	0.69	0.45	0.45	0.23	0.52	0.22
FeO	11.20	5.45	4.39	4.51	14.37	15.47	5.24	10.29	11.40	11.67	9.37
Na_2O	2.52	4.77	3.15	3.62	1.25	2.90	3.16	3.11	3.23	3.15	3.34
K_2O	1.27	3.94	2.15	3.91	0.75	3.16	3.89	2.44	2.63	2.56	2.91
P_2O_5	2.73	1.02	2.40	0.28	6.03	0.62	0.83	1.96	0.58	0.21	1.00
F	0.00	0.41	0.00	0.27	1.28	0.00	0.00	0.00	0.00	0.24	0.00
Cl	0.00	0.00	0.05	0.04	0.00	0.03	0.09	0.00	0.03	0.04	0.00
Total	95.44	97.03	97.91	97.53	95.79	97.26	95.38	96.70	97.62	98.54	96.10

CPX MI—heated in one-atmosphere furnace

	(1)-A*	(1)-B*	(1)-C*	(1)-D*	(1)-E	(1)-F	(1)-G	(1)-H	(1)-I
SiO_2	40.71	40.50	44.72	44.57	47.49	47.79	46.62	44.79	43.54
TiO_2	0.91	0.95	0.44	0.56	1.74	2.12	2.03	2.41	2.77
Al_2O_3	6.36	6.99	10.06	10.23	15.39	14.54	14.43	13.08	13.21
MgO	5.91	5.87	5.94	6.00	6.87	7.06	7.05	9.70	9.54
CaO	19.50	19.50	18.46	18.71	11.91	12.01	12.02	12.17	10.30
MnO	0.51	0.58	0.48	0.53	0.06	0.04	0.05	0.06	0.15
FeO	15.33	15.79	9.91	10.02	7.76	7.91	7.97	9.27	11.12
Na_2O	1.85	1.75	2.45	2.45	2.18	2.16	2.13	2.28	2.86
K_2O	0.55	0.56	0.99	1.01	3.25	3.12	2.96	2.15	2.35
P_2O_5	6.17	6.38	5.48	5.38	0.37	0.44	0.51	0.34	0.52
F	0.05	0.04	0.06	0.06	0.18	0.20	0.20	0.21	0.38
Cl	0.01	0.01	0.02	0.02	0.08	0.08	0.09	0.07	0.09
Total	97.85	98.92	99.00	99.53	97.26	97.46	96.04	96.53	96.81

In parenthesis are number of repeated analyses on a single MI (average shown). Letters refer to corresponding host analysis (Table 1b). Compositions of MI in CPX denoted with an asterisk are contaminated with apatite (corrected compositions are reported in Table 6).

Table 1b
Host crystal compositions

	K-feldspar host			Plagioclase host (stage)												
	A	B	C	A	B	C	D	E	F	G	H	I	L	M	N	O
SiO_2	64.54	63.36	63.78	55.83	55.78	54.84	56.26	56.37	56.60	56.34	55.32	55.32	54.70	55.62	55.55	55.55
TiO_2	0.05	0.05	0.03	0.09	0.02	0.07	0.04	0.10	0.14	0.10	0.05	0.05	0.02	0.02	0.11	0.01
Al_2O_3	19.64	19.65	19.58	28.64	27.42	28.04	26.94	26.75	27.11	27.35	27.67	27.67	27.66	28.29	28.35	27.77
MgO	0.01	0.03	0.02	0.04	0.01	0.03	0.05	0.04	0.03	0.05	0.03	0.03	0.02	0.04	0.02	0.05
CaO	0.69	0.92	1.13	11.13	10.29	10.82	9.28	9.54	9.55	10.12	10.53	10.53	10.88	10.85	10.42	10.15
MnO	0.00	0.01	0.03	0.04	0.03	0.05	0.02	0.11	0.09	0.03	0.04	0.04	0.02	0.03	0.05	0.02
FeO	0.12	0.20	0.33	0.53	0.47	0.31	0.38	0.42	0.48	0.45	0.52	0.52	0.54	0.61	0.51	0.62
Na_2O	3.25	3.18	3.74	4.67	5.04	4.67	5.36	5.33	5.33	5.00	5.01	5.01	4.55	4.86	5.19	5.10
K_2O	9.83	9.45	9.15	0.70	0.85	0.76	1.09	0.97	0.94	0.95	0.79	0.79	0.65	0.61	0.77	0.83
P_2O_5	0.02	0.02	0.03	0.03	0.06	0.07	0.03	0.07	0.05	0.10	0.06	0.06	0.07	0.02	0.02	0.02
F	0.00	1.34	0.07	0.16	0.22	0.11	0.27	0.05	0.23	0.02	0.08	0.08	0.19	0.05	0.11	0.18
Cl	0.02	0.00	0.02	0.01	0.01	0.01	0.04	0.00	0.01	0.01	0.00	0.00	0.02	0.03	0.02	0.02
Total	98.17	98.20	97.88	101.87	100.21	99.79	99.76	99.73	100.56	100.52	100.10	100.10	99.31	101.05	101.11	100.33

	Plagioclase host (stage)											Plagioclase host (furnace)				
	P	Q	R	S	T	U	V	W	X	Y	Z	AA	AB	AD	AE	AH
SiO_2	56.31	55.23	56.75	56.44	56.38	50.84	50.62	51.47	47.65	47.56	46.92	46.71	46.62	45.64	46.06	47.69
TiO_2	0.05	0.07	0.06	0.09	0.04	0.00	0.00	0.12	0.00	0.02	0.20	0.01	0.00	0.00	0.01	0.01
Al_2O_3	27.62	28.28	27.70	27.96	27.47	30.36	30.38	29.64	31.95	32.70	32.30	33.82	33.91	34.24	34.10	32.81
MgO	0.03	0.03	0.04	0.07	0.02	0.05	0.07	0.05	0.13	0.00	0.00	0.10	0.07	0.03	0.04	0.05
CaO	9.89	10.67	9.64	9.76	9.73	13.31	13.03	12.85	15.76	16.59	16.07	16.98	17.20	17.83	17.83	16.15
MnO	0.01	0.07	0.03	0.02	0.07	0.05	0.17	0.26	0.09	0.01	0.11	0.00	0.00	0.00	0.00	0.00
FeO	0.45	0.33	0.32	0.48	0.55	0.58	0.21	0.61	1.98	0.41	0.87	0.59	0.52	0.53	0.56	0.54
Na_2O	5.36	4.88	5.16	5.25	4.40	3.11	3.41	2.90	2.07	1.74	2.05	1.56	1.30	1.13	1.41	2.04
K_2O	0.75	0.70	1.02	0.92	0.92	0.21	0.36	0.39	0.08	0.11	0.17	0.11	0.10	0.09	0.09	0.21
P_2O_5	0.00	0.02	0.04	0.00	0.04	0.00	0.06	0.00	0.00	0.12	0.00	0.03	0.03	0.02	0.04	0.01
F	0.22	0.00	0.10	0.19	0.16	0.00	0.00	0.21	0.00	0.00	0.00	0.00	0.00	0.00	0.00	0.00
Cl	0.01	0.03	0.00	0.03	0.03	0.07	0.00	0.00	0.00	0.04	0.00	0.00	0.01	0.00	0.00	0.01
Total	100.72	100.30	100.87	101.20	99.81	98.58	98.30	98.50	99.71	99.29	98.70	99.92	99.76	99.51	100.14	99.52

	CPX host (stage)								CPX host (furnace)					PF10
	A	B	C	D	E	F	H	I	A	B	D	E	I	
SiO_2	48.65	52.22	48.89	50.50	48.23	50.35	50.44	52.32	51.90	50.70	51.69	48.02	48.758	58.41
TiO_2	1.50	0.39	1.13	0.97	1.40	0.82	0.76	0.39	0.55	0.85	0.50	1.91	1.719	0.78
Al_2O_3	5.22	1.75	4.19	3.87	4.34	3.20	2.39	1.90	2.42	3.84	3.51	5.90	5.423	18.74
MgO	13.26	11.51	11.65	13.47	12.88	12.13	12.41	12.54	13.49	12.85	12.84	13.39	13.615	1.42
CaO	21.37	21.40	21.33	21.21	21.34	21.30	21.97	21.34	22.01	22.14	21.99	21.87	21.913	4.17
MnO	0.27	0.61	0.60	0.40	0.20	0.49	0.47	0.61	0.31	0.37	0.47	0.17	0.164	0.12
FeO	7.71	10.17	9.22	8.14	8.18	8.03	9.39	9.97	8.93	9.07	9.53	7.61	7.528	4.67
Na_2O	0.55	0.49	0.31	0.48	0.45	0.62	0.73	0.55	0.45	0.53	0.52	0.41	0.402	6.64
K_2O	0.03	0.04	0.00	0.02	0.10	0.00	0.00	0.00	0.00	0.00	0.01	0.00	0.000	4.87
P_2O_5	0.00	0.00	0.00	0.05	0.24	0.09	0.18	0.00	0.01	0.02	0.02	0.02	0.026	0.30
F	0.52	0.50	0.15	0.00	0.00	0.19	0.39	0.00	0.00	0.00	0.00	0.00	0.000	NA
Cl	0.00	0.00	0.03	0.00	0.00	0.00	0.06	0.02	0.00	0.01	0.00	0.00	0.006	NA
Total	99.09	99.09	97.48	99.11	97.35	97.21	99.18	99.64	100.07	100.39	101.07	99.29	99.554	100.12

PF10 is Ponza trachyte.

that a 10% increase in volume for an originally 50-μm diameter spherical inclusion would represent less than a 1-μm increase in inclusion diameter. Such a small increase in inclusion size is difficult to detect, either during the heating run or during later petrographic examination.

During early heating runs, it was found that if the sample was heated beyond the temperature at which the last crystal melted (in an attempt to homogenize the vapor bubble), the host crystal containing the inclusions showed considerable melting (in some cases, it melted completely) causing loss of the MI. We believe that this behavior was triggered by melting of some of the ground mass and/or interstitial glass attached to the crystal. It was not possible to completely remove all ground mass (or interstitial glass) from the phenocrysts after their extraction from the thin sections. Attempts to do so using dilute acid solutions regularly resulted in loss of the phenocrysts. In order to preserve the MI, it was decided to stop the experiment and quench the samples after the last solid melted. Consequently, complete homogenization of the inclusions (i.e. disappearance of the vapor bubble) was never achieved.

Failure to achieve complete homogenization of the vapor bubble during heating experiments is likely due to the fact that the pressure in the inclusion is less than the confining pressure during entrapment (Student and Bodnar, 1999). Since volatile solubility in the melt is mainly a function of pressure at the moment of trapping, the lower pressure in the inclusion during laboratory experiments requires heating to higher temperature to dissolve the volatiles back into the melt. We do not have an independent estimate of the

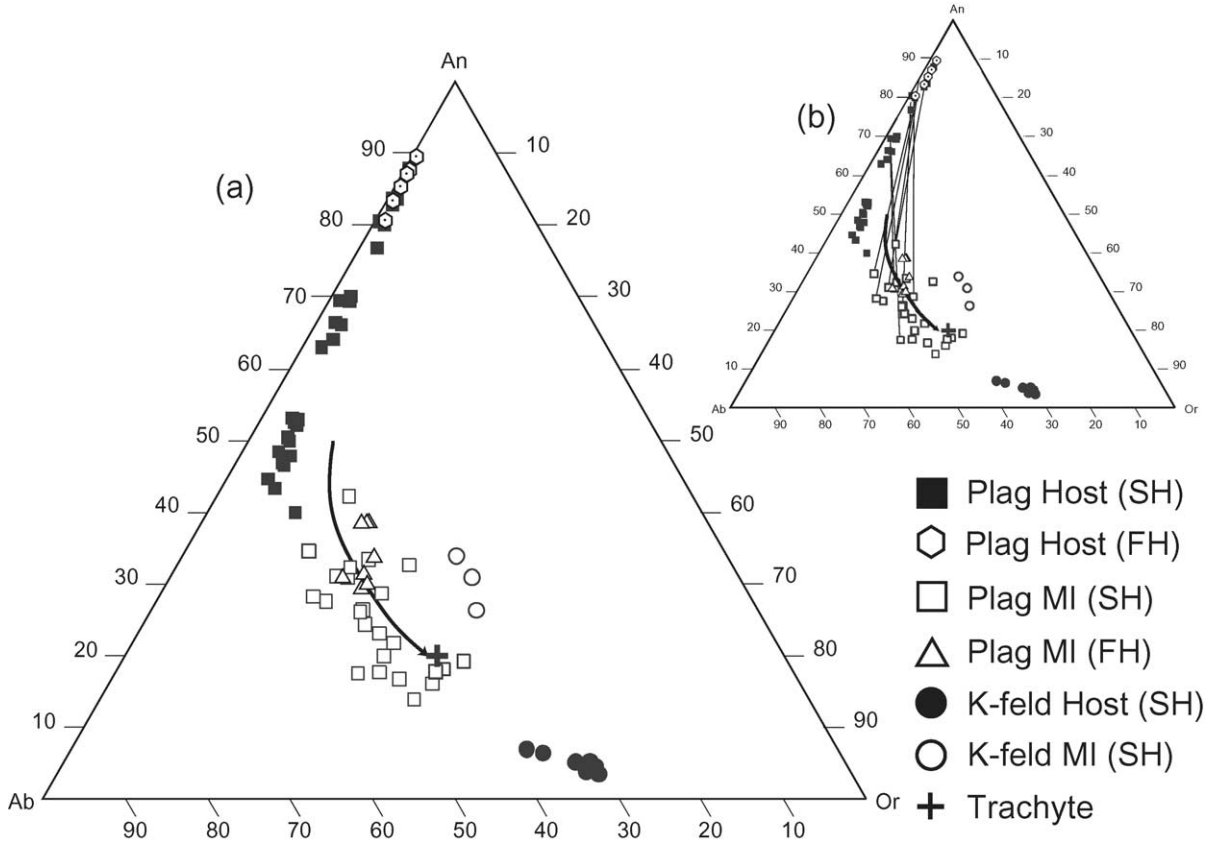

Fig. 4. Compositions of MI and plagioclase host crystals in the system Or–An–Ab. (a) MI define a trend toward the trachyte composition. (b) Tie lines connecting MI compositions with host compositions. Note that increasing Ab content in the host corresponds to MI compositions that are closer to the trachyte composition. Black arrow = melt evolution trend; FH = Furnace Heated, SH = Stage Heated.

trapping pressure, although results from the computer modeling suggest that it did not exceed 100 MPa (see Discussion). Melting temperatures reported here should not be interpreted as trapping temperatures.

The composition (in wt.% oxides) of MI in plagioclase, K-feldspar and pyroxene is shown in Table 1a, while the composition of the associated phenocryst hosts and the Ponza trachyte is shown in Table 1b. Because MI represent the composition of the melt during its evolution (provided one can rule out post-entrapment modifications of MI composition), it is useful to plot MI data on appropriate phase diagrams (i.e. relevant to the phases present in the rock). This allows one to compare analytical results with experimental data available on phase relationships and liquid evolution paths in the system of interest. However, it should be emphasized that because experimentally determined phase diagrams represent systems that are simplifications of natural ones, perfect agreement between natural MI data and experimentally determined phase equilibria is unlikely. For this reason, we also plotted our MI data on conventional Harker variation diagrams to allow comparison with other literature data.

When plotted on the ternary feldspar phase diagram (Ab–An–Or, Fig. 4), the compositions of plagioclase hosts define a broad range from about An_{46} to An_{87} with low but gradually increasing Or content with decreasing An content. K-feldspar host compositions define a more limited range at about Ab_{30} to Ab_{40}, with An < 10%. Compositions of MI in plagioclase define a trend that extends from the host compositions toward the composition of the Ponza trachyte. Noticeably, the compositions of the few MI (3) analyzed in K-feldspar plot toward higher An compositions. In the diopside–albite–anorthite ternary (Di–Ab–An, Fig. 5), compositions of MI in pyroxene lie within the diopside field and extend towards the Cpx-Plagioclase cotectic. While MI compositions appear to evolve from the Di apex toward

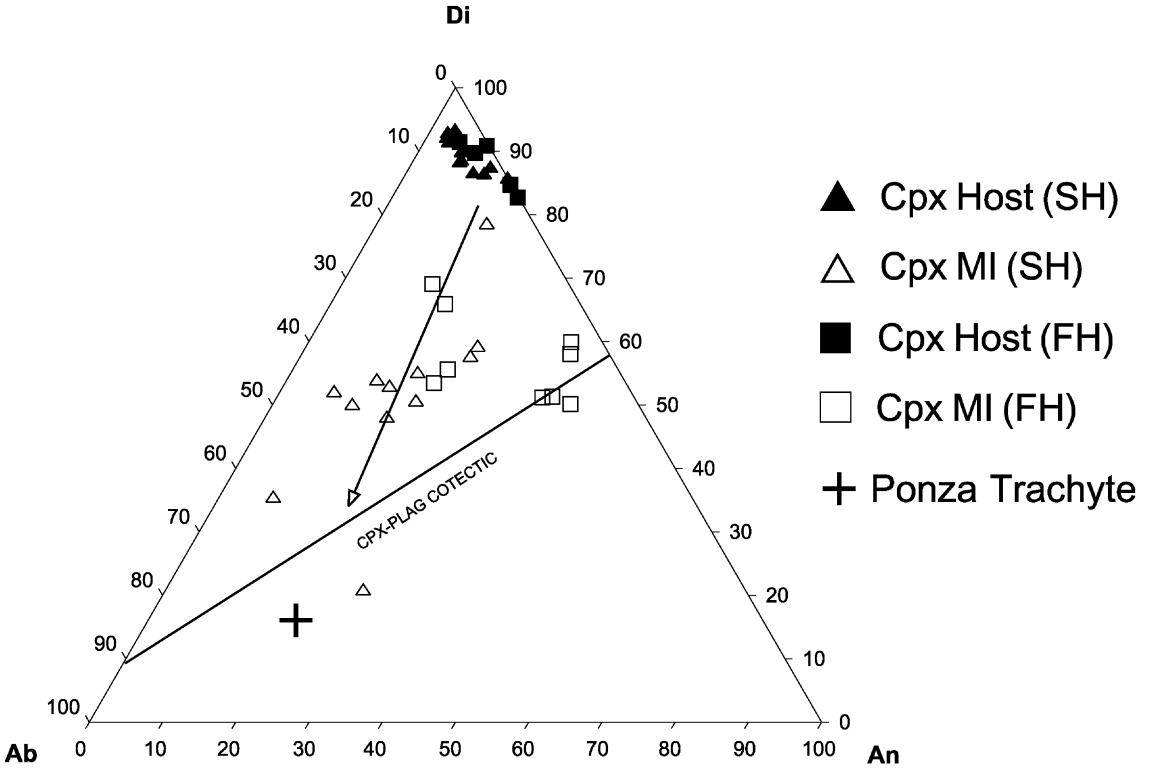

Fig. 5. Compositions of MI and clinopyroxene host crystals in the system An–Di–Ab. The cotectic pyroxene–plagioclase refers to 1 atm pressure (Bowen, 1928); FH = Furnace Heated, SH = Stage Heated. Points were projected from the CaTs ($CaAl_2SiO_6$) apex.

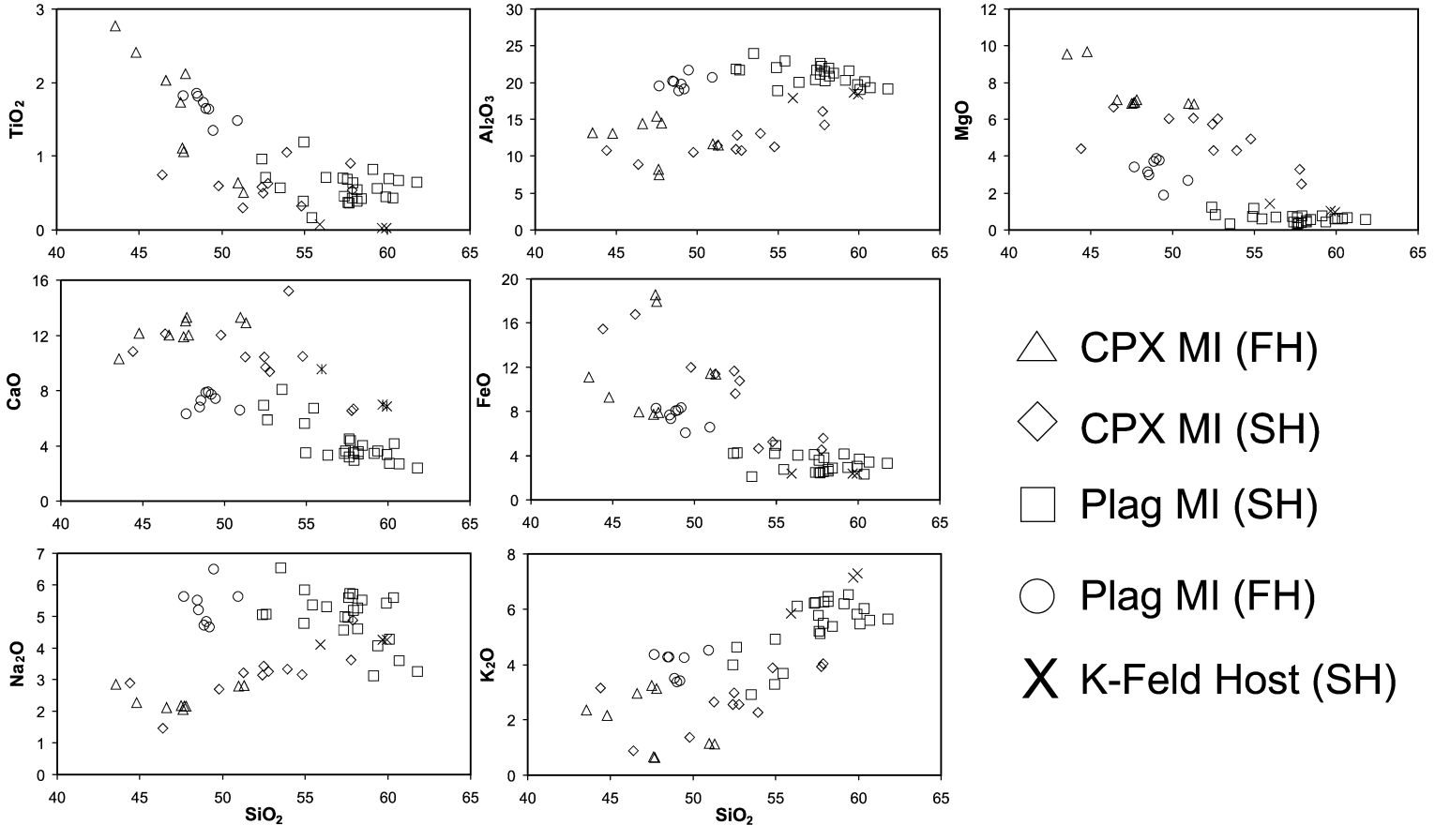

Fig. 6. Harker variation diagrams for all melt inclusions analyzed in this study.

the Cpx-Plagioclase cotectic, a small cluster of MI that where reheated in the 1-atm furnace plot almost on the cotectic itself. These MI are poorer in Na compared with most other MI in clinopyroxene and might be the result of excess remelting of the host.

MI data are plotted on Harker variation diagrams vs. SiO_2 (Fig. 6). While all plots show substantial scatter in the MI data, general trends with increasing SiO_2 are easily recognizable. The data show a decrease in TiO_2, MgO, CaO and FeO with increasing SiO_2, and an increase in Al_2O_3, Na_2O and K_2O as SiO_2 increases. At SiO_2 concentrations greater than about 50–55 wt.%, FeO, and to a lesser extent TiO_2 and MgO, become constant and low. In this same range, the concentrations of Na_2O and Al_2O_3 begin to decrease with increasing SiO_2. CaO and K_2O show a continuous decrease and increase, respectively, with increasing SiO_2. Compositions of MI heated in the microscope stage and MI heated in the 1-atm furnace partially overlap, both for the clinopyroxene and plagioclase groups, as do data for clinopyroxene and plagioclase as a whole. MI in K-feldspar always plot at the high-SiO_2 end for all elements and overlap with plagioclase MI data. The presence of MI in clinopyroxene with low-SiO_2 content and high-CaO/Na_2O is notable. The compositions of these inclusions have been altered by accidentally trapped apatite, as indicated by the high-P_2O_5 content (Table 1a). When recalculated after subtracting the apatite contribution (assuming that all P represents apatite and using the stoichiometric formula: $Ca_5[PO_4]_3OH$), these compositions become similar to other MI in clinopyroxenes, and the CaO/Na_2O ratio decreases (Table 6).

6. Discussion

A fundamental assumption in every melt inclusion study is that MI are samples of the melt trapped during crystallization of the host crystal. This assumption has been questioned by some workers who suggest that the slow diffusion of components in the melt can induce the formation of boundary layers surrounding growing crystals (Watson et al., 1982; Bacon, 1989). According to this model, incompatible elements are enriched in the boundary layer, whereas compatible elements are depleted. Melts within the boundary layer thus do not represent the composition of the bulk melt and, if trapped as a MI, would provide misleading information on the composition of the melt.

Based on detailed studies of melt inclusions, it is believed that the effect of chemical gradients within the boundary layer on melt inclusion compositions is negligible for inclusions ≥ 50 μm in diameter (Lu et al., 1995) and is insignificant for inclusions greater than 25 μm (Lowenstern, 1995; Anderson, 1974). Recent work by Thomas et al. (2001) documented the absence of boundary layer effects in melt inclusions trapped in coeval zircon, allanite, quartz and plagioclase from the Toba tuffs. Most of the inclusions used in this study were 25 μm or more in diameter and no correlation between size and composition was observed for the smallest inclusions analyzed. Our interpretation of these observations is that boundary layer processes had little or no effect on melt inclusion composition.

Assuming that MI are samples of the original melt trapped during crystallization, the compositions of melt inclusions necessarily represent points on the liquid line of descent for the host rock at the conditions existing in the magma chamber. It follows that a logical approach is to compare the analytical data obtained from MI with phase relationships in systems where the principal phases present in the host rock are considered. In our case, two systems are of major interest: orthoclase–anorthite–albite (i.e. the ternary feldspar system, OAA, as shown in Fig. 4) and anorthite–diopside–albite (ADA, as shown in Fig. 5). As noted above, phase diagrams represent systems that are simpler than real magmatic ones and may not accurately reflect melt evolution in natural systems. As a consequence, we have also presented our data on classic Harker variation diagrams (Fig. 6).

There has been extensive experimental and theoretical work on the OAA system (Bowen and Tuttle, 1950; Tuttle and Bowen, 1950; Yoder et al., 1957; Seck, 1971; Barron, 1976; Ghiorso, 1984; Furhman and Lindsley, 1988; Wen and Nekvasil, 1994), and the fundamental phase relationships are fairly well known at different pressures. Less information is available for the ADA system. The basic phase relationships in the ADA system were determined by Bowen (1928), who documented the existence of two primary crystallization fields at 10^5 Pa. Barron (1972), using a thermodynamic approach, confirmed Bowen's earlier

experimental findings. Lindsley and Emslie (1968) showed that the cotectic boundary between the two primary crystallization fields moves toward compositions richer in anorthite at higher pressure (>15 MPa).

When plotted in the OAA system, compositions of MI inclusions from the Ponza trachyte define a fractional crystallization path that extends from a "basaltic" liquid composition towards the trachyte composition (Fig. 4). Note that compositions of melt inclusions heated slowly in the heating stage and those heated rapidly in the vertical furnace overlap, indicating that slow heating did not significantly affect the melting behavior or the melt composition as had been reported by Sobolev et al. (1980). As shown schematically in Fig. 7 (modified from Cox et al., 1979), the evolution of a basaltic liquid of composition (B) through fractionation of calcic plagioclase of composition (a) defines a curved path which trends toward the cotectic. At the cotectic, the liquid, now trachytic in composition (P), starts to precipitate K-feldspar of composition (e) in addition to plagioclase with composition (b). The three inclusions analyzed in K-feldspar plot away from the inclusions in plagioclase (Fig. 4) which suggests that they did not trap a melt that was co-precipitating plagioclase and K-feldspar. However, the compositions of MI in plagioclase and K-feldspar are similar when plotted on Harker variation diagrams (Fig. 6). Hence, we infer

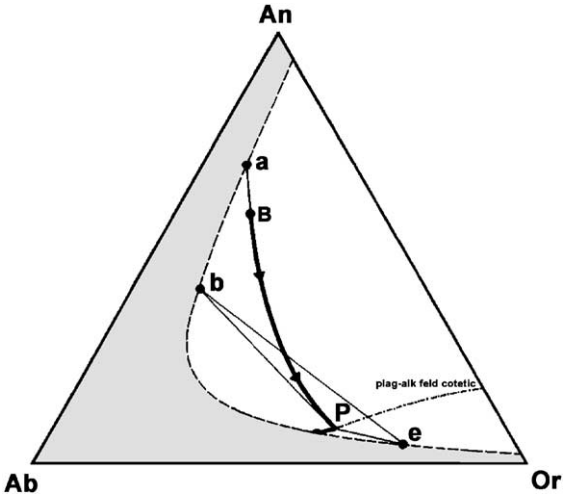

Fig. 7. Evolution of a basaltic melt composition during fractional crystallization in the system orthoclase–albite–anorthite–H_2O at low pressure. See text for discussion (modified after Cox et al., 1979).

that the differences shown in Fig. 4 are at least partly the result of distortion introduced by projecting the data onto the ternary phase diagram.

Compositions of melt inclusions in clinopyroxene have been plotted in the ADA system (Fig. 5). According to the phase relationships in this system, these inclusions trapped a liquid, which was precipitating a diopsidic pyroxene. This caused the liquid to move away from the diopside apex and towards the pyroxene–plagioclase cotectic curve, a behavior compatible with that observed in the OAA system. This path is represented schematically with a straight line in Fig. 5, but the actual liquid line of descent (LLD) was likely more complicated. The cotectic precipitation of clinopyroxene and plagioclase, although suggested by the trend in Fig. 5 and the partial overlap of MI data for clinopyroxene and plagioclase in Fig. 6, cannot be unequivocally proved due to the large variability of MI data when plotted in the ADA system.

A precise LLD cannot be constructed owing to the scatter of the data (Figs. 4 and 5) and the lack of more rigorous experimental constraints on phase relationships in the system albite–anorthite–orthoclase–Diopside (AAOD). Nonetheless, a plot of all MI data in this tetrahedron (Fig. 8) is consistent with the interpretation that the parent liquid which produced the trachyte evolved from the Di corner towards the An–Ab–Or join, probably reaching a point along the path where a diopsidic clinopyroxene co-precipitated with an anorthitic feldspar. Once the liquid, now closer in composition to a trachyte than the original basaltic parent, reached the An–Ab–Or side of the tetrahedron, the path moved toward the two-feldspar solvus, crossed it and started to fractionate K-feldspar together with plagioclase.

Data from MI in feldspar have been plotted in the ternary system OAA, as constructed by Barron (1976) and based on data from Seck (1971) at 100 MPa (Fig. 9a). Also shown are compositions of the MI host crystals, and the composition of the Ponza trachyte. MI from high-Ca plagioclase (An_{63} to An_{87}) plot closer to the An–Ab side, whereas MI data from low-Ca plagioclase (An_{46} to An_{55}) cluster near the trachyte composition, together with MI data from K-feldspar. The data from K-feldspar plot between the An_{50} and An_{65} icophase lines (which represent the composition of K-feldspar that would be in equili-

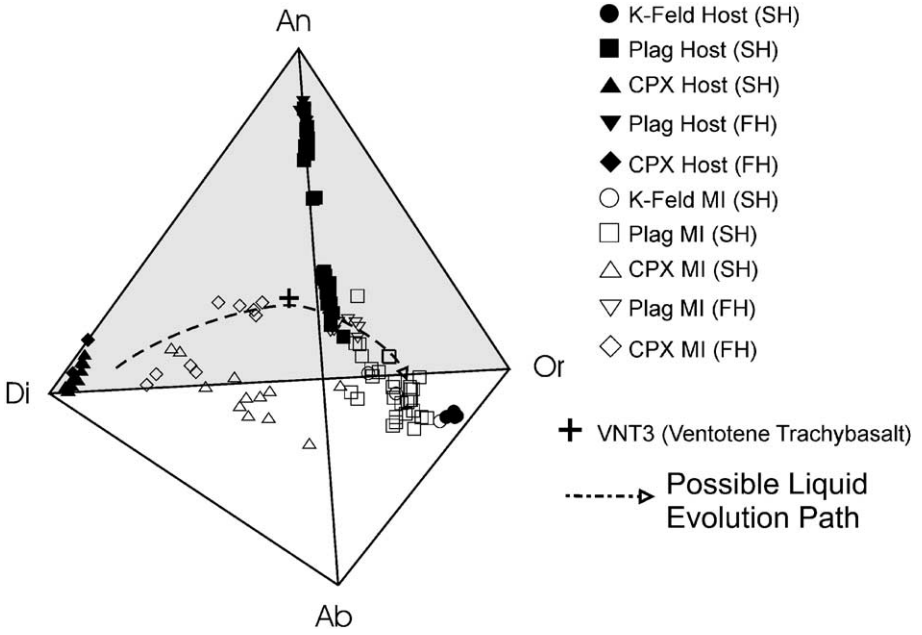

Fig. 8. Compositions of MI and host crystals (plagioclase, K-feldspar and clinopyroxene) plotted in the tetrahedron Or–An–Ab–Di.

brium with plagioclase of a particular An content at a certain temperature) indicating that they co-precipitated with the low-Ca (An_{50} to An_{55}) plagioclase. Moreover, the composition of the Ponza trachyte plots almost exactly on the consolute line (which marks the co-precipitation of K-feldspar and plagioclase). For comparison, we also plotted our data on the 200-MPa phase diagram (Fig. 9b; Barron, 1976). At this higher pressure, the consolute line moves towards the An–Ab join and there is poorer agreement between our data and experimental phase relationships, suggesting that pressures during melt entrapment were closer to 100 MPa than 200 MPa. On this diagram, K-feldspars plot on the An_{40} icophase line and the Ponza Trachyte is far away from the consolute line. All these observations taken together strongly support the hypothesis that the Ponza trachyte evolved from a basaltic parent through fractional crystallization in a shallow magma chamber and that this process played a major role in its evolution, albeit not the only one.

The suggestion that the origin of the trachytic magmas at Ponza is the result of low-pressure differentiation processes in shallow reservoirs is not new (Metrich et al., 1988), and recent geophysical data confirm the existence of an intensely magnetized body that "could represent the remnant of a shallow magma chamber" (Orsi et al., 1999). To further test this hypothesis and to identify a possible parent melt for the Ponza trachyte, we have carried out theoretical geochemical modeling using the computer program MELTS (Ghiorso and Sack, 1995). We selected an alkali olivine basalt from the nearby Ventotene island (Table 2, VNT3 in: Bellucci et al., 1999) for our starting composition in the MELTS model. The Ponza trachyte and VNT3 are thought to be products of the same magmatic system, and radiometric dating indicates similar ages for these two units (Metrich et al., 1988).

In our model, we constrained the pressure at 100 MPa, as suggested by the agreement between our MI compositions, host crystal compositions and bulk rock data and the phase relations in the Ab–An–Or phase diagram as shown in Fig. 9a. As a starting temperature, we selected 1250 °C, because this temperature is slightly above the highest temperature required to attain complete melting of crystallized melt inclusions and hence is likely above the liquidus for this composition. This was confirmed by our runs with MELTS. However, as long as the starting temperature is above the liquidus, this temperature choice has no

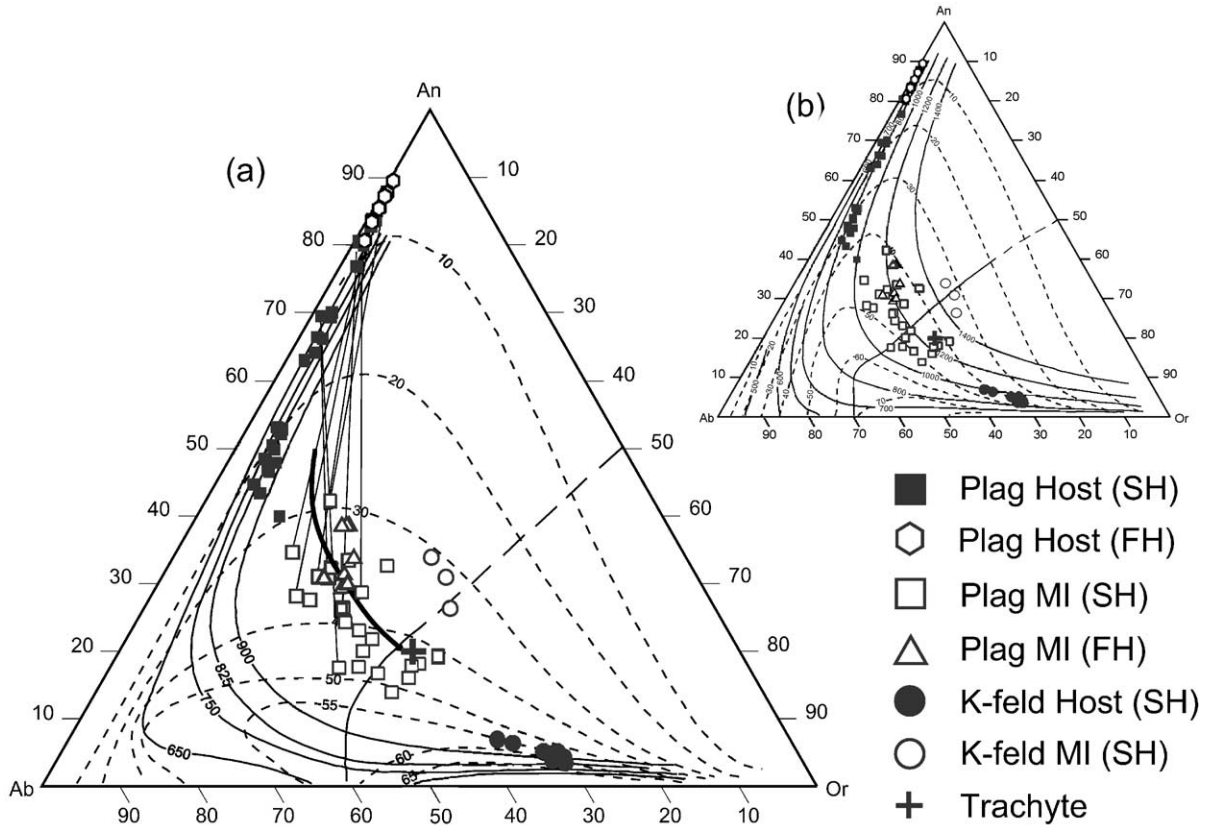

Fig. 9. Comparison of measured compositions of MI and host feldspars with compositions predicted by phase relationships in the system Or–An–Ab at 100 MPa (a) and 200 MPa (b). Dashed lines = icophases; solid lines = feldspar solvus labeled in degrees Celsius. Numbers on icophases represent %Ab in plagioclase co-precipitating with K-feldspar.

effect on the model results, because MELTS calculates the highest liquidus temperature purely on the basis of the starting composition, pressure and oxygen fugacity. For practical purposes, we could have selected any temperature at which we can consider our starting composition to be above the liquidus and the results would not change. In the model, the temperature was decreased in 5 °C steps. Oxygen fugacity was constrained along the QFM buffer, assuming that most igneous rocks of this composition equilibrate within a few log units of this buffer (Haggerty, 1976). However, since a few log unit variations in oxygen fugacity could have a large effect on the liquid line of descent, we also investigated the effect of oxygen fugacity on the predicted evolution of the melt.

MELTS predicts a liquidus temperature of 1170 °C, at which point the liquid starts precipitating clinopyroxene and plagioclase. Clinopyroxene and plagioclase are joined by olivine at 1165 °C, by spinel at 1115 °C and by K-feldspar at 1030 °C. Olivine leaves the liquidus at 1025 °C, immediately after K-feldspar crystallization begins. Apatite appears at 1000 °C and biotite at 895 °C. The model results are summarized in Tables 2 and 3. The evolution of the liquid along the liquid line of descent in the ternary feldspar system is shown in Fig. 10b, together with the predicted compositions of the precipitating feldspars. In Fig. 10a, the liquid evolution path is compared to the MI data.

Results from the MELTS model, and analytical data from minerals and melt inclusions, agree in many respects, but not in all. MELTS model results and the MI data describe a similar crystallization trend and compositions of feldspars, and the order in which

Table 2
Variation of liquid composition during cooling as predicted by MELTS

	Start. comp.	*T*, °C							
	VNT3	1170	1120	1070	1020	970	920	870	820
		Liq. comp.							
SiO_2	48.83	48.95	49.88	55.7	57.98	57.75	57.3	55.77	52.45
TiO_2	1.19	1.22	1.67	1.16	1.04	1.03	0.59	0.34	0.12
Al_2O_3	18.54	18.42	18.55	18.7	18.13	18.15	18.03	16.66	14.28
Fe_2O_3	1.5	1.56	1.81	1.11	0.72	0.55	0.55	0.61	0.79
FeO	7.39	7.51	8.66	4.48	2.55	1.81	1.7	1.69	1.76
MnO	0.15	0.15	0.2	0.27	0.36	0.71	1.17	2.38	3.94
MgO	5.76	5.8	3.35	1.67	1.07	0.9	0.72	0.49	0.2
CaO	10.55	10.4	7.47	5.05	4.13	3.73	3.13	2.63	2.27
Na_2O	2.32	2.35	3	3.74	4	4.91	6.34	9.06	13.04
K_2O	3.02	3.09	4.56	6.82	8.12	7.53	6.19	4.04	2.12
P_2O_5	0.25	0.26	0.38	0.59	0.86	0.91	0.81	0.9	1.2
H_2O	0.3	0.31	0.46	0.7	1.04	2.02	3.47	5.42	7.85

VNT3: Ventotene trachybasalt.

phases crystallize (Tables 3 and 4, Fig. 10a and b). However, whereas MELTS predicts a continuous range of plagioclase compositions (Fig. 10b), data from the trachyte show two gaps in the plagioclase composition, corresponding to An_{72}–An_{78} and An_{56}–An_{63}. The gaps in measured compositions of these zoned plagioclases are likely the result of the limited number of analysis.

The MELTS model results and the MI data disagree on two points. MELTS does not reproduce the actual composition of the pyroxenes (Table 4). However, it is known that the model poorly reproduces pyroxene equilibria (Yang et al., 1996). Additionally, the evolution trend of the liquid composition predicted by MELTS (i.e. the Liquid Line of Descent—LLD) and the one shown by MI data are clearly different. LLD defined by MELTS during plagioclase-only crystallization is displaced toward compositions richer in An and Or, compared to the trend defined by the MI analyses (Fig. 10b). There are a number of possible explanations for these differences, some of which are considered below.

Table 3
Phases assemblages on liquidus during cooling as predicted by MELTS

T, °C	Phases on the liquidus							%Cryst.
1170	Cpx (Di)	Plag (An)						2.36
1165	Cpx	Plag	Ol (Fo)					7.03
1115	Cpx	Plag	Ol	Sp (Mag)				37.79
1030	Cpx	Plag	Ol	Sp	K-felds			65.82
1025	CPx	Plag		Sp	K-felds			68.83
1000	Cpx	Plag		Sp	K-felds	Ap		78.83
895	Cpx	Plag		Sp	K-felds	Ap	Bi	93.38
875		Plag		Sp	K-felds	Ap	Bi	95.5

Magmatic systems are complex, and many different physical and chemical factors affect the chemical evolution of magmas. However, theoretical models generally cannot consider all of the many possible combinations that might occur in natural systems, and it is not always possible to determine analytically with a high degree of accuracy all of the parameters that go into a model.

For example, we have chosen VNT3 as the starting composition because it belongs to the same magmatic system as the Ponza trachyte. An artificial composition might have produced a closer match with our MI data, but we intended to illustrate how MI data can be combined with a theoretical model in order to constrain the parameters that control magmatic processes in natural systems containing real rocks.

Pressure in the magma chamber can significantly affect the LLD. Geologic information suggests a shallow magma chamber at Ponza, and after comparing MI data with phase equilibria (Fig. 9a and b) determined from experimental data (Seck, 1971), we selected a pressure of 100 MPa for our model. Higher pressures show poorer agreement between model and

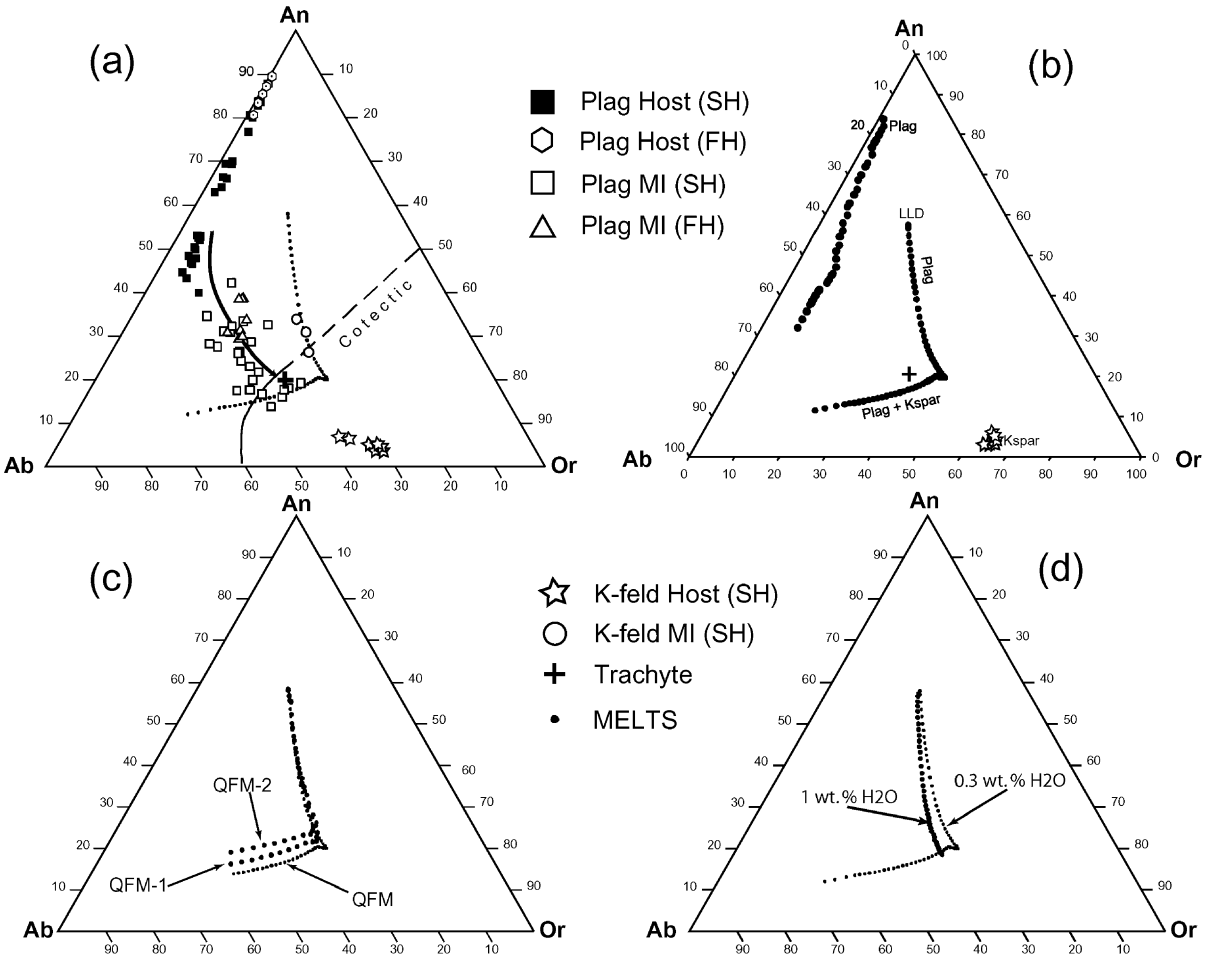

Fig. 10. (a) Comparison between the liquid line of descent (LLD) predicted by MELTS (black dots) and the trend indicated by MI data (black arrow). Also shown are host crystal analysis and the cotectic for 100 MPa. (b) Plagioclase, K-feldspar composition and LLD generated by MELTS at 100 MPa. (c) LLD generated by MELTS at 100 MPa and different f_{O_2} buffer values. (d) LLD generated by MELTS at 100 MPa and different H_2O contents.

MI predictions. The oxygen fugacity during MI entrapment is not well constrained, and we selected QFM for our model. Changing f_{O_2} one or two log units below the QFM buffer has an insignificant effect on the plagioclase-only part of the LLD, whereas the co-precipitation of K-feldspar and plagioclase was shifted to slightly lower temperatures and compositions richer in anorthite (Fig. 10c). The H_2O content of the melts is not well known, and we used a value of 0.3 wt.% for the starting melt in our model. Increasing the initial water content in the VNT3 sample to 1 wt.% (Fig. 10d) caused a slight shift of the plagioclase-only part of the LLD toward compositions richer in Ab. However, this part of the LLD still differs from the trend defined by MI data. A further increase of the

Table 4
Comparison of observed and predicted compositions of minerals in the Ponza trachyte

Mineral	Composition range		
	MELTS		Trachyte
Pyroxene	1170–1030 °C	Di [54–43]	Di [69–50]
Plagioclase	1170–875 °C	An [83–32]	An [88–40]
K-feldspar	1030–875 °C	Or [64–63]	Or [66–55]

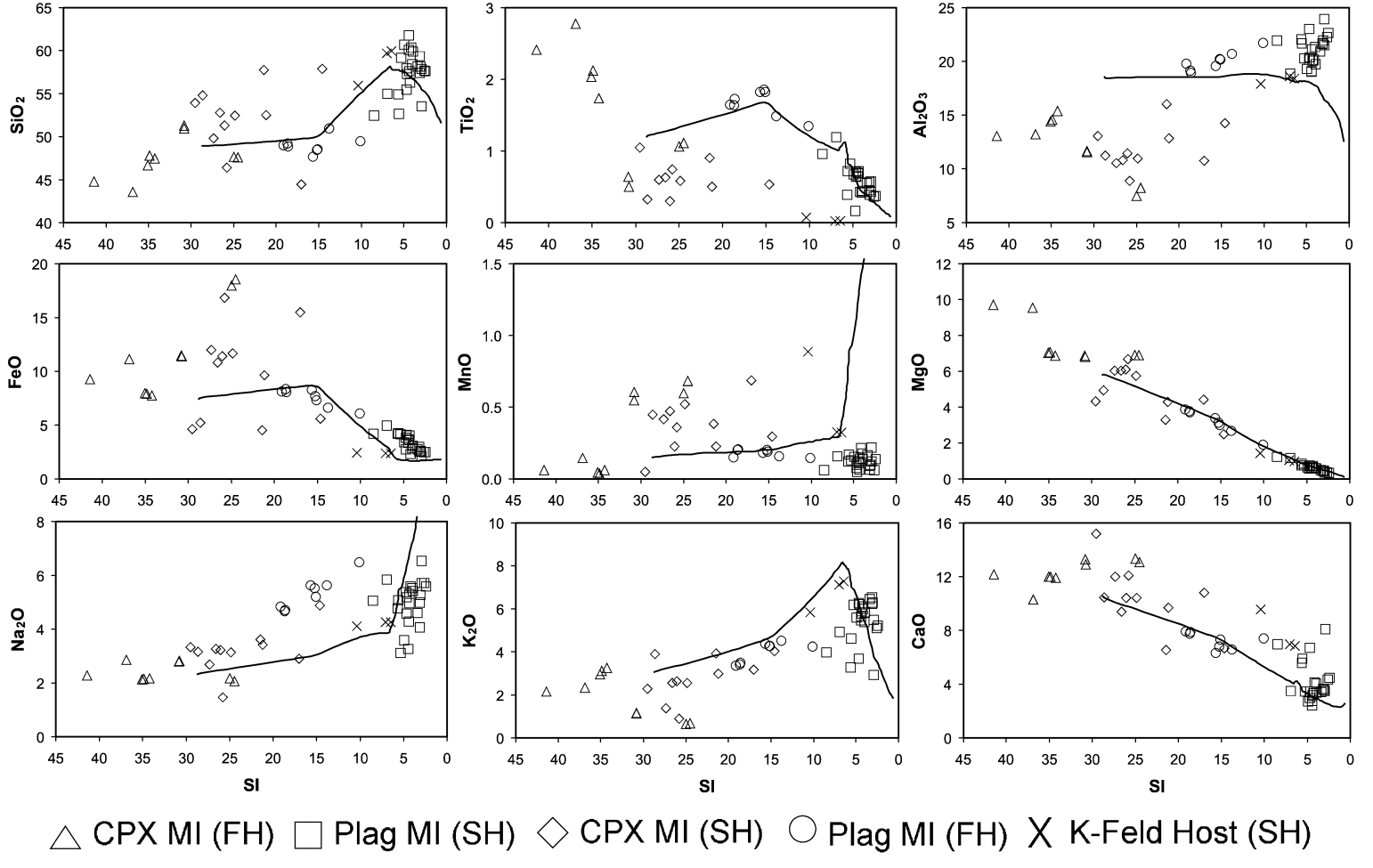

Fig. 11. Compositions of MI plotted vs. solidification index (SI). Solid line = oxide evolution trend predicted by MELTS (starting from VNT3 composition).

initial water content would have produced an even greater shift of the LLD predicted by MELTS towards the MI trend, but we have no evidence of high water content in the melts (i.e. no evidence of magmatic aqueous inclusions).

Concentrations of oxide components from melt inclusions are plotted against the Solidification Index ($SI=[100 \times MgO/(MgO + FeO + Fe_2O_3 + Na_2O + K_2O)]$) together with the MELTS-modeled evolution of the Ventotene AOB (Fig. 11). Although there is some scatter of the data, MI analyses agree with the modeled trends for SiO_2, FeO, MnO, MgO, Na_2O, K_2O and CaO, with major discrepancy only for TiO_2 and Al_2O_3. The behavior of Al_2O_3 is especially anomalous when compared with the trend produced by MELTS. A possible explanation is that melt inclusions in more evolved plagioclase were modified by excess remelting of the host during heating. Indeed late plagioclase hosts (i.e. those formed at lower temperatures) would be more susceptible to melting at the temperatures of the remelting experiments. We have calculated the effect of excess host remelting by subtracting 25% of the host composition from MI analysis and report a few sample calculations in Table 5. It is worth noting that these plots also show that some MI in clinopyroxene apparently record the melt evolution before the point where our modeling starts. In fact even after correction for apatite contamination, some MI in clinopyroxene still have SI>30 (Table 6).

Based on the data from MI and the results from MELTS, we suggest a genetic link between the trachyte and the Ventotene alkali olivine basalt (VNT3), consistent with earlier interpretations. As is clearly shown in (Figs. 4, 5, 9 and 10) and Table 3, fractional crystallization of VNT3 at 100 MPa produces both the phases found in the trachyte and a crystallization trend parallel to the one recorded by MI, whereas the data in Fig. 11 confirm the close match between the compositional data obtained by MI and that predicted by MELTS modeling. The difference between the crystallization path obtained by MI data and the one produced by MELTS as plotted in Fig. 10a could be explained by the following:

(1) As shown in Fig. 11, VNT3 is genetically linked to the Ponza trachyte but it is not the primary magma that generated the trachyte. This parental magma likely had a different composition represented by the MI compositions in pyroxene and it might have followed a different LLD.
(2) MELTS was designed to reproduce melt evolution in a multi-component system (Ghiorso and Sack, 1995) and plots in Fig. 10 represent an extrapolation of the results obtained through MELTS modeling to a three-component system. This forces the mathematical model into unfamiliar territory and, while preserving the general trend for the LLD, could explain the discrepancy observed in Fig. 10a.

Table 5
MI in Plagioclase corrected for excess remelting of the host

	MI in plagioclase after subtraction of 25% host									
	(1)-A	(1)-B	(2)-C	(2)-D	(1)-E	(1)-F	(1)-G	(2)-H	(1)-I	(1)-L
SiO_2	58.55	58.98	60.78	61.76	64.01	62.63	60.52	59.22	59.54	58.60
TiO_2	0.92	0.85	1.08	0.92	0.83	0.86	0.72	0.50	0.72	0.60
Al_2O_3	17.88	17.88	17.77	16.54	16.67	16.87	19.75	20.09	18.76	19.80
MgO	0.96	1.00	1.00	0.81	0.75	0.87	0.57	0.58	0.64	0.59
CaO	0.89	0.52	0.97	0.59	0.00	0.42	1.49	1.28	1.02	1.24
MnO	0.05	0.12	0.15	0.14	0.13	0.17	0.08	0.11	0.21	0.12
FeO	5.33	4.98	5.44	4.81	4.30	4.41	3.77	3.27	3.52	3.18
Na_2O	4.60	5.26	2.62	3.96	2.60	3.05	3.77	5.36	4.51	5.17
K_2O	8.15	8.11	8.02	6.97	7.24	7.23	8.41	8.14	8.39	8.14
P_2O_5	0.36	0.37	0.42	1.10	1.00	1.04	0.32	0.19	0.27	0.13
F	0.14	0.12	0.28	0.19	0.27	0.24	0.23	0.43	0.24	0.01
Cl	0.23	0.20	0.23	0.01	0.01	0.01	0.30	0.30	0.27	0.18
Total	98.06	98.40	98.76	97.78	97.81	97.82	99.92	99.48	98.08	97.76

Table 6
MI in CPX corrected for apatite contamination

	MI in CPX after correction for apatite contamination									
	Heated with Linkam and Vernadsky stages						Heated in one-atmosphere furnace			
	(1)-A	(1)-B	(1)-C	(1)-E	(1)-H	(1)-M	(1)-A	(1)-B	(1)-C	(1)-D
SiO_2	49.78	57.87	53.92	46.38	52.76	52.50	47.67	47.61	51.29	50.96
TiO_2	0.60	0.54	1.05	0.74	0.63	0.50	1.06	1.11	0.50	0.63
Al_2O_3	10.53	14.26	13.07	8.89	10.80	12.87	7.45	8.21	11.54	11.69
MgO	6.04	2.48	4.31	6.66	6.02	4.30	6.92	6.90	6.81	6.86
CaO	12.01	6.67	15.18	12.10	9.39	9.69	13.32	13.05	12.90	13.29
MnO	0.41	0.30	0.05	0.36	0.47	0.23	0.59	0.68	0.55	0.61
FeO	12.00	5.58	4.65	16.82	10.80	9.60	17.96	18.57	11.37	11.45
Na_2O	2.70	4.88	3.34	1.46	3.26	3.43	2.16	2.06	2.81	2.80
K_2O	1.36	4.03	2.28	0.88	2.56	2.98	0.65	0.66	1.13	1.15
F	n.a.	0.42	n.a.	1.50	n.a.	n.a.	0.06	0.04	0.07	0.07
Cl	n.a.	n.a.	0.05	0.00	n.a.	n.a.	0.02	0.01	0.03	0.02
Total	95.44	97.03	97.91	95.79	96.70	96.10	97.85	98.92	99.00	99.53
CaO/N_2O	4.45	1.37	4.54	8.30	2.88	2.83	6.15	6.34	4.59	4.75
SI	27.35	14.62	29.54	25.81	26.60	21.19	24.99	24.49	30.79	30.83

(3) There are uncertainties connected to the MI data, which might be due to under-melting or over-melting of the plagioclase and clinopyroxene hosts or to other magmatic processes superimposed on the fractional crystallization process. These factors cannot be quantified with the available data.

7. Conclusions

The origin of the Ponza trachyte was investigated by combining compositional data obtained from MI with compositional trends predicted by theoretical modeling using the program MELTS. MI were reheated to obtain an homogeneous glass before analysis. This was done using two different techniques, slow heating in a heating stage and fast heating in a vertical furnace, with the purpose of identifying possible of effects of heating rates on MI compositions. No detectable effect was found. MI data were compared with known phase relations in the ternary feldspar and anorthite–diopside–albite systems to constrain the physical parameters used in the modeling.

MI data are consistent with melt evolution from a basaltic parent via a fractional crystallization process, which was controlled mainly by crystallization of pyroxene and feldspars, but cannot exclude substantial contributions from other magmatic processes. These data, in conjunction with the results from MELTS, are consistent with a genetic link between the Ponza trachyte and the coeval and co-magmatic alkali olivine basalts (VNT3) on the nearby Ventotene Island.

Acknowledgements

The authors wish to thank Giuseppe Rolandi and Annamaria Lima for their help and guidance in collecting rock samples in Ponza and Mark Ghiorso for his help with MELTS. Our gratitude goes also to Charles Mandeville for his advice on the Electron Microprobe analyses and Jim Webster for his help with the furnace experiments and the discussions, which improved the final version of the paper. Reviews of an earlier version of this paper by John Holloway, Alex Sobolev, Leonid Danyushevsky, Roger Nielsen and Maria Luce Frezzotti helped in improving the final manuscript. The reviews provided many useful suggestions to improve the interpretation and presentation. Any errors and inconsistencies that remain are solely the responsibility of the authors. **[RR]**

References

Anderson, A.T., 1974. Evidence for a picritic, volatile-rich magma beneath Mt. Shasta, California. J. Petrol. 15, 243–267.

Bacon, C.R., 1989. Crystallization of accessory phases in magmas by local saturation adjacent to phenocrysts. Geochim. Cosmochim. Acta 53, 1055–1066.

Barberi, F., Gasparini, P., Innocenti, F., Villari, L., 1973. Volcanism of the Southern Tyrrhenian Sea and its geodynamic implications. J. Geophys. Res. 78, 5221–5232.

Barron, L.M., 1972. Thermodynamic multicomponent silicate equilibrium phase calculations. Am. Mineral. 57, 809–823.

Barron, L.M., 1976. A comparison of two models of ternary excess free energy. Contrib. Mineral. Petrol. 57, 71–81.

Bassi, G., Sabadini, R., Rebai, S., 1997. Modern tectonic regime in the Tyrrhenian area: observations and models. Geophys. J. Int. 129, 330–346.

Bellucci, F., Lirer, R., Munno, R., 1999. Geology of Ponza, Ventotene and Santo Stefano islands (with a 1:15,000 scale geological map). Acta Vulcanol. 11 (2), 197–222.

Boccaletti, M., Guazzone, G., 1972. Evoluzione Paleogeografica e Geodinamica del Mediterraneo: I. Bacini Marginali. Mem. Soc. Geol. Ital. 13, 162–169.

Bodnar, R.J., Bethke, P.M., 1984. Systematics of stretching of fluid inclusions: I. Fluorite and sphalerite at 1 atmosphere confining pressure. Econ. Geol. 79, 141–161.

Bowen, N.L., 1928. The Evolution of the Igneous Rocks. Princeton Univ. Press, Princeton, NJ.

Bowen, N.L., Tuttle, O.F., 1950. The system $NaAlSi_3O_8$–Kal Si_3O_8–H_2O. J. Geol. 58 (5), 489–511.

Conte, A.M., Dolfi, D., 2002. Petrological and geochemical characteristics of Plio-Pleistocene volcanics from Ponza Island (Tyrrhenian Sea, Italy). Mineral. Petrol. 74, 75–94.

Cox, K.G., Bell, J.D., Pankhurst, R.J., 1979. The Interpretation of Igneous Rocks. Unwin Hyman, London. 450 pp.

Danyushevsky, L.V., McNeill, A.W., Sobolev, A.V., 2002. Experimental and petrological studies of melt inclusions in phenocrysts from mantle-derived magmas: an overview of techniques, advantages and complications. In: Hauri, E.H., Kent, A.J.R., Arndt, N. (Eds.), Melt inclusions at the millennium; toward a deeper understanding of magmatic processes. Chem. Geol., vol. 183, pp. 5–24.

Frezzotti, M.L., 2001. Silicate-melt inclusions in magmatic rocks: application to petrology. Lithos 55, 273–299.

Furhman, M.L., Lindsley, D.H., 1988. Ternary-feldspar modeling and thermometry. Am. Mineral. 73, 201–215.

Ghiorso, M.S., 1984. Activity/composition relations in the ternary feldspars. Contrib. Mineral. Petrol. 87 (3), 282–296.

Ghiorso, M.S., Sack, R.O., 1995. Chemical mass transfer in magmatic processes: IV. A revised and internally consistent thermodynamic model for the interpolation and extrapolation of liquid–solid equilibria in magmatic systems at elevated temperatures and pressures. Contrib. Mineral. Petrol. 119, 197–212.

Haggerty, S.E., 1976. Opaque mineral oxides in terrestrial igneous rocks. In: Rumble, D., III (Ed.), Oxide minerals, vol. 3. Mineralogical Society of America Short Course Notes. 200p.

Halter, W., Pettke, T., Heinrich, C.A., Rothen-Rutishauser, B., 2002. Major to trace element analysis of melt inclusions by laser-ablation ICP-MS: methods of quantification. In: Hauri, E.H., Kent, A.J.R., Arndt, N. (Eds.), Melt inclusions at the millennium; toward a deeper understanding of magmatic processes. Chem. Geol., vol. 182, pp. 63–86.

Hari, K.R., Santosh, M., Chatterjee, A.C., 1991. Primary silicate-melt inclusions in olivine phenocrysts from the Pavagad Igneous Suite, Gujarat. J. Geol. Soc. India 37, 343–350.

Laubscher, H.P., 1975. Plate boundaries and microplates in Alpine history. Am. J. Sci. 275, 865–876.

Lavecchia, G., Stoppa, F., 1996. The tectonic significance of Italian magmatism: an alternative view to the popular interpretation. Terra Nova 8, 435–446.

Lindsley, D.H., Emslie, R.F., 1968. Effect of pressure on the boundary curve in the system Diopside–Albite–Anorthite. Carnegie Inst. Washington, Year Book 66, 479–480.

Locardi, E., 1982. Individuazione di Strutture sismogenetiche dall'esame dell'evoluzione vulcano-tettonica dell'Appennino e del Tirreno. Mem. Soc. Geol. Ital. 34, 569–596.

Lowenstern, J.B., 1994. Chlorine, fluid immiscibility and degassing in peralkaline magmas from Pantelleria, Italy. Am. Mineral. 79, 353–369.

Lowenstern, J.B., 1995. Applications of silicate-melt inclusions to the study of magmatic volatiles. In: Thompson, J.F.H. (Ed.), Fluids and Ore Deposition. Mineral. Assoc. Canada, Short Course Series, vol. 23, pp. 71–99.

Lu, F., Anderson, A.T., Davis, A.M., 1995. Diffusional gradients at the crystal/melt interface and their effect on the compositions of melt inclusions. J. Geol. 103, 591–597.

Metrich, N., Santacroce, R., Savelli, C., 1988. Ventotene, a potassic quaternary volcano in Central Tyrrhenian Sea. Rend. Soc. Ital. Mineral. Petrol. 43, 1195–1213.

Nielsen, R.L., Crum, J., Bourgeois, R., Hascall, K., Forsythe, L.M., Fisk, M.R., Christie, D.M., 1995. Melt inclusions in high-An plagioclase from the Gorda Ridge: an example of the local diversity of MORB parent magmas. Contrib. Mineral. Petrol. 122, 34–50.

Nielsen, R.L., Michael, P.J., Sours-Page, R., 1998. Chemical and physical indicators of compromised melt inclusions. Geochim. Cosmochim. Acta 62 (5), 831–839.

Orsi, G., Patella, D., Piochi, M., Tramacere, A., 1999. Magnetic modeling of the Phlegraean Volcanic District with extension to the Ponza archipelago, Italy. J. Volcanol. Geotherm. Res. 91, 345–360.

Patacca, E., Sartori, R., Scandone, P., 1990. Tyrrhenian basin and Apenninic Arcs: kinematic relations since late Tortonian times. Mem. Soc. Geol. Ital. 45, 425–451.

Pozzuoli, A., 1988. Mineralogy, geochemistry and origin of alteration products in the Pontian Archipelago (Italy): 1. The Genesis of the Ponza Bentonite. 10th Conference on Clay Mineralogy and Petrology, Ostrava, pp. 89–98.

Qin, Z., Lu, F., Anderson Jr., A.T., 1992. Diffusive reequilibration of melt and fluid inclusions. Am. Mineral. 77, 565–576.

Raia, F., Webster, J.D., De Vivo, B., 2000. Pre-eruptive volatile contents of Vesuvius magmas: constraints on eruptive history and behavior: I. The medieval and modern interplinian activities. Eur. J. Mineral. 12, 179–193.

Roedder, E., 1979. Origin and significance of magmatic inclusions. Bull. Minéral. 102, 487–510.

Roedder, E., 1984. Fluid inclusions. Mineral. Soc. Am. Rev. Min. 12 (646 pp.).

Savelli, D., Wezel, F.C., 1979. Morfologia e stile tettonico del Bacino Tirrenico. Atti Conv. Sc. Naz. P.F. Oceanografia Fondi Marini CNR Roma 2, 729–738.

Scandone, P., 1980. Origin of the Tyrrhenian Sea and Calabrian Arc. Boll. Soc. Geol. Ital. 98, 27–34.

Seck, H.A., 1971. Koexistierende Alkalifelspate und Plagioklase im System $NaAlSi_3O_8$–$KalSi_3O_8$–$CaAl_2Si_2O_8$–H_2O bei Temperaturen von 650 °C bis 900 °C. Neues Jahrb. Mineral. Abh. 115, 315–345.

Sinton, C.W., Christie, D.M., Coombs, V.L., Nielsen, R.L., Fisk, M.R., 1993. Near-primary melt inclusions in anorthite phenocrysts from the Galapagos Platform. Earth Planet. Sci. Lett. 119, 527–537.

Skirius, C.M., Peterson, J.W., Anderson Jr., A.T., 1990. Homogenizing rhyolitic glass inclusions from the Bishop Tuff. Am. Mineral. 75, 1381–1398.

Sobolev, A.V., 1996. Melt inclusions in minerals as a source of principal petrologic information. Petrology 4, 228–239.

Sobolev, A.V., Dmitriev, L.V., Barsukov, V.L., Nevsorov, V.N., Slutsky, A.B., 1980. The formation conditions of high magnesium olivines from the mono-mineral fraction of Luna-24 regolith. In: Criswell, P.R., Merrill, R.B. (Eds.), Igneous processes and remote sensing. Proceedings of the Lunar and Planetary Science Conference. Lunar and Planetary Institute, Houston, TX, United States (USA).

Stanley, D.J., Wezel, F.C., 1985. Geological Evolution of the Mediterranean Basin. Springer-Verlag, New York. 589 pp.

Student, J.J., Bodnar, R.J., 1999. Synthetic fluid inclusions: XIV. Microthermometric and compositional analysis of coexisting silicate melt and aqueous fluid inclusions trapped in the haplogranite–H2O–NaCl–KCl system at 800 °C and 2000 bars. J. Petrol. 40, 1509–1525.

Thomas, R., Webster, J.D., 2000. Strong tin enrichment in a pegmatite-forming melt. Miner. Depos. 35, 570–582.

Thomas, J.B., Shimizu, N., Sinha, A.K., Bodnar, R.J., 2000. Melt inclusions in zircon as recorders of melt evolution in crystallizing granitic plutons. Geol. Soc. Am., Program Abstr., A398.

Thomas, J.B., Bodnar, J.B., Shimizu, N., Chesner, C., 2001. The role of boundary layers during entrapment of melt inclusions: evidence from the Toba Tuffs Sumatra, Indonesia. EOS Trans. AGU 82 (47) (Fall Meeting Suppl. Abs. V32D-1014).

Turco, E., Zuppetta, A., 1998. A kinematic model for the Plio-Quaternary evolution of the Tyrrhenian–Apenninica System: implications for rifting processes and volcanism. J. Volcanol. Geotherm. Res. 82, 1–18.

Tuttle, O.F., Bowen, N.L., 1950. High-temperature albite and contiguous feldspars. J. Geol. 58 (5), 572–583.

Ulrich, M.R., Bodnar, R.J., 1988. Systematics of stretching fluid inclusions: II. Barite at one atmosphere confining pressure. Econ. Geol. 83, 1037–1046.

Watson, E.B., Sneering, M.A., Ross, A., 1982. Diffusion of dissolved carbonate in magmas: experimental results and applications. Earth Planet. Sci. Lett. 61, 346–358.

Wen, S., Nekvasil, H., 1994. Solvcalc: an interactive graphics program package for calculating the ternary feldspar solvus and for two-feldspar geothermometry. Comput. Geosci. 20 (6), 1025–1040.

Yang, K., Bodnar, R.J., 1994. Magmatic-hydrothermal evolution in the "bottoms" of porphyry copper systems: evidence from silicate melt and aqueous fluid inclusions in granitoid intrusions in the Gyeongsang Basin, South Korea. Int. Geol. Rev. 36, 608–628.

Yang, H., Kinzler, J.K., Grove, T.L., 1996. Experiments and models of anhydrous, basaltic olivine–plagioclase-augite saturated melts from 0.001 to 10 Kbar. Contrib. Mineral. Petrol. 124, 1–18.

Ylagan, R.F., Altaner, S.P., Pozzuoli, A., 1996. Hydrothermal alteration of a rhyolitic hyaloclastite from Ponza Island, Italy. J. Volcanol. Geotherm. Res. 74, 215–231.

Yoder, H.S., Stewart, D.B., Smith, J.R., 1957. Ternary feldspars. Carnegie Inst. Washington, Year Book 56, 207–214.